國立臺灣大學理學院化學研究所

碩士論文

Graduate Institute of Chemistry

College of Science

National Taiwan University

Master Thesis

高空氣穩定性二維類核殼結構錫鈣鈦礦光致發光材料

High air stability two-dimensional core shell like structure tin-based perovskite photoluminescence material

胡育愷

Yu-Kai Hu

指導教授：周必泰 博士

Advisor: Pi-Tai Chou, Ph.D.

中華民國 108 年 7 月

July 2019

doi:10.6342/NTU201903018

國立臺灣大學碩士學位論文
口試委員會審定書

高空氣穩定性二維類核殼結構錫鈣鈦礦光致發光材料

High Air Stability Two-Dimensional Core Shell like Structure Tin-Based Perovskite Photoluminescence Material

本論文係 **胡育愷** 君（學號 R06223163）在國立臺灣大學化學系完成之碩士學位論文，於民國 108 年 7 月 19 日承下列考試委員審查通過及口試及格，特此證明。

口試委員：

（簽名）

（指導教授）

系主任、所長 （簽章）

doi:10.6342/NTU201903018

誌謝

很感謝周老師這兩年的指導，讓我自由地發揮。也很感謝各位學長姐、同學、還有學弟妹的幫忙和陪伴。最後，祝大家未來都有好的發展。

doi:10.6342/NTU201903018

摘要

錫基鈣鈦礦是一種很有前景的半導體材料，且最具前瞻性的鉛替代品。根據理論和實驗，錫基鈣鈦礦表現出較窄的帶隙和與鉛類似的光電特性。然而，錫基鈣鈦礦的空氣穩定性差，阻礙了實際應用的發展。許多團隊已經做出了很多努力，例如添加額外的氯化亞錫 (SnF_2) 作為補償劑或者將維度從三維降到二維鈣鈦礦以防止四價錫的產生。因此，合成了具有化學式 TEA_2SnI_4（TEA = 噻吩基乙基銨）的新型鈣鈦礦納米板，通過將具有強化學相互作用的硫氰酸銨（NH4SCN）添加劑引入到錫基鈣鈦礦中，可以顯著提高其空氣穩定性和光致發光性能。在優化的條件下，我們的結果顯示錫基鈣鈦礦的空氣穩定性實際上得到改善。此外，光致發光量子產率（PLQY）可達 22 %。

關鍵字: 錫基鈣鈦礦、無鉛鈣鈦礦、低維度鈣鈦礦、二維材料、發光材料

doi:10.6342/NTU201903018

Abstract

Tin-based perivskite is a promising semiconductor material and is the most forward-looking candidates of lead alternative. According to theory and experiment, tin-based perovskite exhibits narrower band gap and comparable photoelectric properties to lead analog. However, the poor oxidative stability of tin-based perovskite has hindered the development for real application. Many groups have contributed a lot of efforts, such as adding extra SnF_2 as compensator or decreasing the dimensionality form three-dimensional to two-dimensional perovskite to prevent Sn^{4+} generation. Hence, new tin perovskite nanoplates with chemical formula TEA_2SnI_4 (TEA = thienylethylammonium) is synthesized and its air stability and photoluminescence property can be significantly enhanced by introducing ammonium thiocyanate (NH_4SCN) additive with strong chemical interactions to Sn^{2+} into 2D tin-based perovskites. Under optimized condition, our results show that the air stability of tin perovskite is actually improved. Besides, the photoluminescence quantum yield (PLQY) can reach to 22%.

Key words: Tin-based perovskites, Lead-free perovskites, Low-dimensional perovskites, Two-dimensional material, Photoluminescence material

doi:10.6342/NTU201903018

Content

doi:10.6342/NTU201903018

doi:10.6342/NTU201903018

doi:10.6342/NTU201903018

List of Figures

doi:10.6342/NTU201903018

doi:10.6342/NTU201903018

doi:10.6342/NTU201903018

doi:10.6342/NTU201903018

List of Tables

doi:10.6342/NTU201903018

Chapter 1 Perovskites Introduction

1.1 Background

Hybrid perovskites originated from the mine of calcium titanate ($CaTiO_3$) are discovered and identified by Gustav Rose in 1839 and named in honor of Lev Perovski (1792−1856). Although it was known and vigorously promoted at the applications of magnetic and optical/electronic in the late 20^{th} century, hybrid perovskites have been extremely developed and focused in recent two decades. Metal halide perovskite is an attractive material with semiconductor features, including ferro-electricity, superconductivity, and magnetoresistance properties. Besides, metal halide perovskites show high absorption coefficients (e.g. CH_3PbI_3 has the order 10^4 cm^{-1}), narrow full width at half maximum (FWHM), tunable direct energy band gap, low trap density (lower than 10^{16} cm^{-3}), high charge-carrier mobility (exceeding 10 $cm^2V^{-1}s^{-1}$), and long minority carrier diffusion lengths (1 μm and greater).

As mentioned above, perovskites have many good optoelectronic properties. At the part of light-to-electricity field, these material have opened a new route for low-cost manufacture solar cell. At 2009, Miyasaka et al. added $CH_3NH_3PbI_3$ ($MAPbI_3$) and $CH_3NH_3PbBr_3$ ($MAPbBr_3$) with dye-sensitized solar cell (DSSC), and they received the

doi:10.6342/NTU201903018

power conversion efficiency (PCE) 3.8 % and 3.1 %, respectively.[1] Recently, Michael Grätzel's group introduced a method for preparing perovskite films of high electronic quality and implemented it for the fabrication of perovskite solar cell with excellent performance and certified PCE attaining 21 %.[2] More recently, the power conversion efficiency (PCE) is more than 23 %,[3] which can compete with best-known thin film technologies such as CIGS (copper indium gallium selenide material alloy), CdTe, or amorphous Si and close to monocrystalline silicon (25 %).

On the other hand, at the part of electricity-to-light field, at 1995, S. Saito et al. reported a layered structured halide perovskite ($(C_6H_5C_2H_4NH_3)_2PbI_4$, PEA_2PbI_4) to create light-emitting diodes (LEDs) which operated at liquid nitrogen temperature.[4] In 2014, Richard H. Friend et al. published a room temperature halide perovskite LEDs structure at Nature Nanotechnology.[5] In 2015, Lee et al. reported the first efficient perovskite LEDs (EQE ~ 8.5 %).[6] Recently, Jianpu Wang and Wei Huang et al. successfully made in 2016 and got a light-emitting diode with an external quantum efficiency of 11.6 % through the use of two-dimensional structure of lead perovskite NFPI (the amine salts used were 1-naphthylmethylamine iodide, NMAI and formamidinium iodide, FAI), making further progress towards commercialization.[7] In the past six years, researches of perovskites optical source have been more intensified.

Besides, due to the outstanding optoelectronic properties and tunability of halide

doi:10.6342/NTU201903018

perovskites, the applications concerned are not only solar cells and LEDs but also photodetectors,[8] X-ray detectors,[9-10] and lasers.[11]

Chapter 2 Structure

2.1 Three-Dimensional Perovskites

Three-dimensional (3D) halide perovskites have the formula $A^{I}B^{II}X_3$. In general, 3D halide perovskites consist of a simple arrangement of divalent B-site cations bridged by halide anions (X = Cl^-, Br^-, I^-), and form a 3D corner-sharing octahedral network. The perovskite is a crystal structure which the monovalent cation (green) occupies in the lattice center, and the metal cation (blue) is arranged in the octahedral hole (corner) of the crystal lattice, as well as the monovalent anion (red) is located on the side of the crystal lattice (as shown in Figure 1).

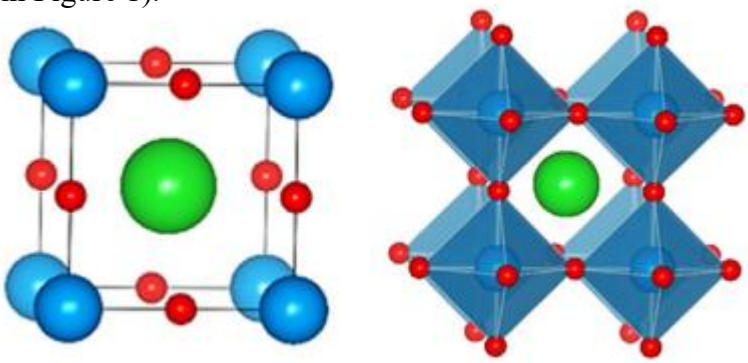

Figure 1.1 3D perovskites structure. A site is monovalent cation (green), B site is the metal cation (blue), and X site is the monovalent anion (red).

doi:10.6342/NTU201903018

The metal halide octahedral structure may twist or rotate with each other, which is similar to oxide perovskites. These structures have been named and established to illustrate their differences.[12-13] Due to remarkable optoelectronic properties, the 3D perovskites with Pb^{2+} occupying B site have been received widespread attention by the world in this decade. Other B site metals, such as Sn^{2+},[14] Ge^{2+},[15] Cd^{2+},[16] and Mn^{2+},[17] have been incorporated into the halide octahedral crystal lattice. Besides, the appearance of double perovskites composed by two metals increases flexibility at the B site. Double perovskites are combined with mono- and trivalent cations or tetravalent cations and vacancies in an ordered array at B sites, which still maintain an average 2+ charge. Generally, the A site of 3D perovskites is occupied by a small monovalent metal cation such as K^+, Rb^+, or Cs^+ or small monovalent organic cations (e.g. methylammonium ($CH_3NH_3^+$),[18-19] formamidinium ($CH(NH_2)NH_2^+$)[20]) called organic-inorganic hybrid perovskites.

2.2 Two-Dimensional Perovskites

At the case of 3D perovskites, the A-site cation is located at the cuboctahedra cavity and can't exceed the critical size of the cavity because the original A-site cation is too small.[21-22] Changing to larger A-site cations can exceed the critical size and form lower-dimensional 2D, one-dimensional (1D), or zero-dimensional (0D) derivatives. Just like

doi:10.6342/NTU201903018

3D perovskites, the substitutions at B and X sites of 2D perovskites are allowed, while a much alternative of A-site cations can be localized at cuboctahedra cavity and can form diverse template perovskites.

2.2.1 Connectivity of the Inorganic Layer

The characteristic of 2D perovskites is non-3D inorganic flat sheets of corner-sharing octahedral, which means that this network structure can be described from the 3D perovskites ABX_3 structure by reducing its dimension. That is, this layered structure can be obtained by cutting the ABX_3 structure in a plane perpendicular to the (001)-oriented.[23]

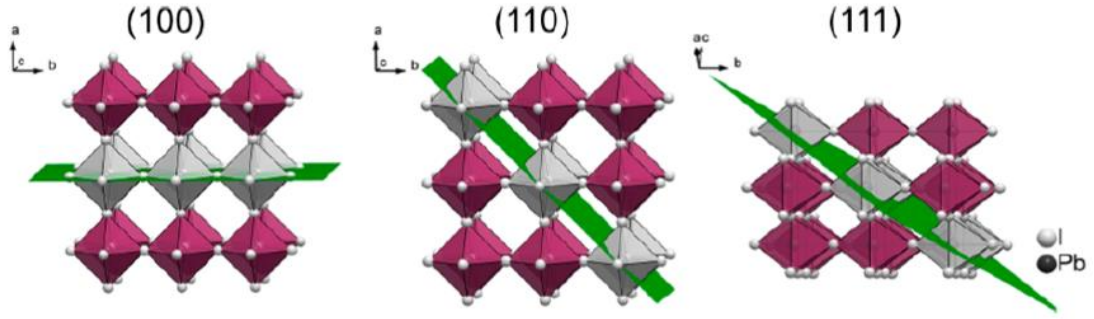

Figure 2.1 2D perovskite is described from the 3D cubic perovskite lattice by cutting the latter along typical crystallographic planes: (100), (110), and (111).

Another way to describe the (100)-oriented layered perovskites consists is to remove neutral $B^{II}X_2$ units from the ABX_3 structure or to substitute $B^{II}X_1^+$ units by organic cations. Not only the (100)-oriented but also (110)-oriented[24] and less (111)-oriented[25] layered perovskites are derived from 3D perovskites, which had been reported at *Chemical*

doi:10.6342/NTU201903018

Review by D. Mitzi in 2016.[23] Besides, there are more complicated corrugate layered structures, which cannot be simply defined by the above methods.[26-28] These complex arrangement 2D perovskites can be prepared by solution-state self-assembly processes with different organic cations. The A-site cation plays an important role in the structural orientation of the two-dimensional perovskites. Vitally, diverse structure types can exhibit significantly different optical properties.

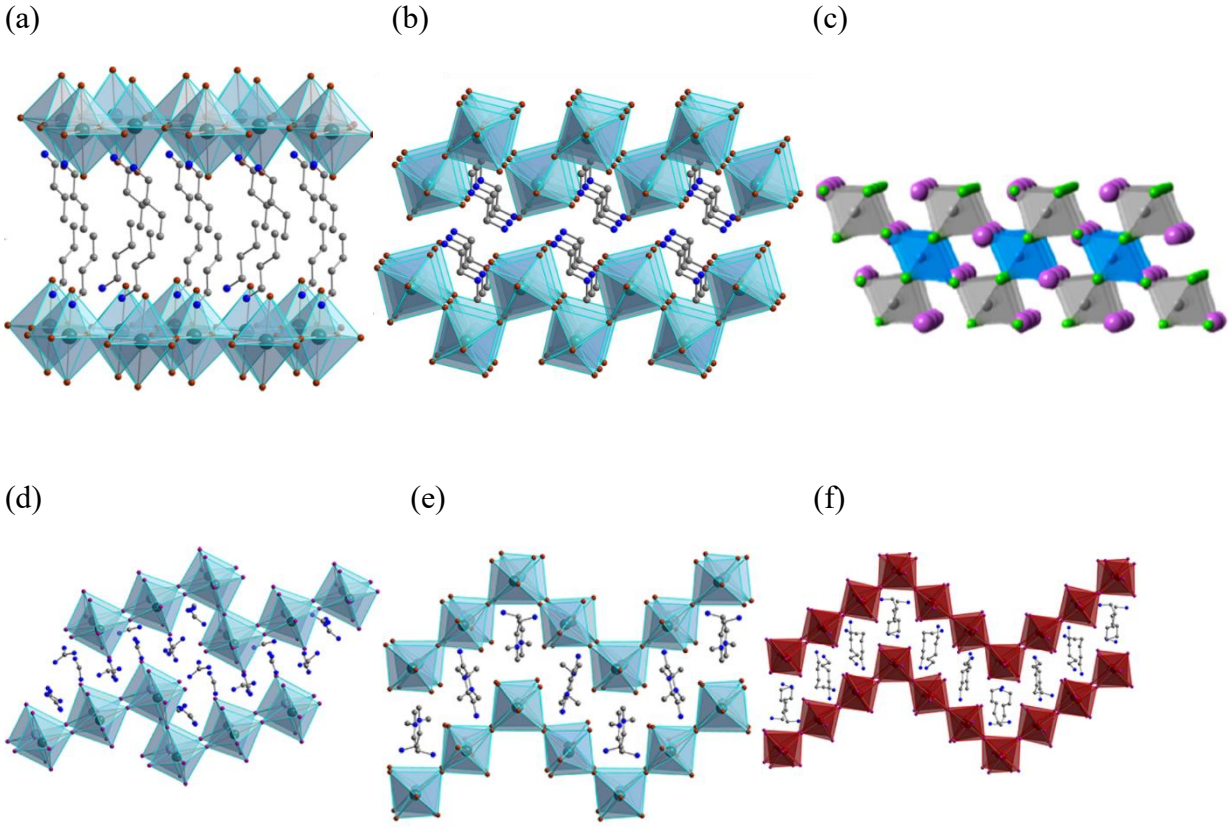

Figure 2.2 Crystal structures of (a) (100) perovskite $(BA)_2PbBr_4$ ($BA = C_4H_9NH_3^+$),[29] (b) (110) perovskite (N-MEDA)$PbBr_4$ (N-MEDA = N1-methylethane-1,2-diammonium),[24] (c) (111) perovskite $Cs_4CuSb_2Cl_{12}$,[25] (d) (FA)(GUA)PbI_4 ($FA = CH(NH_2)_2^+$; GUA = $C(NH_2)_3^+$),[26] (e) α - (DMEN)$PbBr_4$ (DMEN = 2-(dimethylamino)ethylamine),[27] and (f)

doi:10.6342/NTU201903018

α -(1,5-PDA)SnI_4 (1,5-PDA = 1,5-pentanediammonium).[28]

2.2.2 Structural Distortions of the Inorganic Layer

Actually, relating to the ideal cubic 3D perovskite lattice, the inorganic sheet of layered perovskite exhibits significant distortions. The most common distortions include the unequal coordination bond length of the equatorial plane and vertical plane B-X, the bond angle of X-B-X is deviating 90° or 180° and tilting between metal halide octahedral. These distortions can be varied widely by different A-site cations in spite of compositing with the same B-site cation and X-site halide. Mitzi et al. found a significant change at the isomers of 4-Fluoro (4-FPEA) and 3-Fluoro (3-FPEA) forming 2D tin-base perovskites, which Sn-I-Sn angle of layered perovskites formed from 4-FPEA and 3-FPEA is 156.375° and 154.16°, respectively.[30] In 2005, Knutson et al. summarized a series 2D tin-based perovskites formed by different ammonium salts, and their Sn-I-Sn bond angle and band gap. They observed that the band gap as well as the bandwidth of the valence and conduction bands of the $(RNH_3)_2SnI_4$ hybrid semiconductor perovskites can be subtly influenced by variation in the structural requirements of the organic cation.[31] Different packing arrays between the bilayer of organic were resulting in these variations, and therefore, this phenomenon highlights that the importance of A-site cation in the inorganic sheet structure distortion. Hydrogen-bonding influences,[30, 32-35] the organic

doi:10.6342/NTU201903018

cation steric demands,[36] alkylammonium head charge density,[31, 37] and organic cation penetration depth[38] have been emphasized and considered the important factors.

2.2.3 Thickness of the Inorganic Layer

In the initial (100) -oriented perovskites, the inorganic templates always compose single layered metal halide octahedron, called monolayer perovskite, which thickness is the metal halide octahedron. However, a series of intermediate structures exist between 3D perovskites and monolayer perovskites. Adjusting the proportion of small and large A-site cations can vary the thickness of inorganic layer.[39] The general formula of (100)-series perovskites are $A'_2A_{n-1}B_nX_{3n+1}$, where the small cations (A) occupy the inner inorganic templates octahedral cavities, and the larger cations (A') localize and insert at the outer inorganic templates octahedral cavities. n is the number of octahedral layers, which can be quantified as the thickness of the layer, and both (110)[40] and (111)[25] thicker inorganic layers can be synthesized. As the number n increases, the optical property of multilayer perovskites approaches to 3D perovskites ($n = \infty$ layers).[41-42]

2.2.4 The A Site

At the case of 2D perovskites, the A-site cations are usually organoammonium cations, which terminal ammonium groups have hydrogen bonds with halides of the inorganic layers. The most common organoammonium cations are monoammonium

doi:10.6342/NTU201903018

cations (e.g. R-NH_3^+; R = aliphatic or aromatic group), forming an organic bilayer in the perovskites structure, or diammonium cations (^+H_3N-R-NH_3^+; R = aliphatic or aromatic group), forming an organic monolayer in the perovskites structure. Also, there are some reports indicated that alkali metal cations can form 2D perovskites. The luminescence properties of 2D perovskites are greatly influenced by the choice of A-site cation. The organic and inorganic layers should be mutual templates like multi-layer sandwich.

2.2.5 The B Site

The different B-site cations greatly determine the 2D perovskites electronic structure and furthermore, luminescence properties. The most common divalent B-site cation is Pb^{2+},[43] besides, there are some alternative divalent B-site cations, including Sn^{2+},[44] Ge^{2+},[45] Cu^{2+},[46] Mn^{2+},[47] Fe^{2+},[48] and Eu^{2+}.[49] In addition, Mitzi et al. successfully synthesized a 2D perovskite containing Bi^{3+}, where the excess positive charge is balanced by B-site vacancies.[50] The double perovskite framework offers another route to explore the more possibility of different B-site cations combination. By using this strategy, Guloy and co-workers successfully synthesized (001)-orientation layered double perovskites, which combined Au^+ and Au^{3+}.[51] Lately, Solis-Ibarra and co-worker reported the double perovskites composed by Cu^{2+} and Sb^{3+} with (111)-orientation feature.[25] And recently, Karunadasa et al. reported n =1 and 2 (001) orientation double perovskites with Ag^+ and

doi:10.6342/NTU201903018

Bi^{3+} at B site.[52]

2.2.6 The X Site

The X site of layered hybrid perovskites basically involve I^-, Br^-, or Cl^- halides, though, in some case the 2D perovskites contain F^- anions (e.g. K_2MgF_4). The different halides directly and significantly affect the band gap, and mixed-halide compositions can be able to tune the band gap smoothly and get the variation of photoluminescence energy across the visible region even ultra-visible region.[53-55] However, due to the steric requirements of coordinating six halides around the B-site cations, some B-site cations cannot form perovskite structures with every halide. Besides, there are also several cases of 2D halide perovskites including pseudohalide, such as SCN^-[56] and I_3^-.[51]

Chapter 3 Electric Confinement

Variation the dimensions of perovskites strongly affect the electronic structure. The thickness of the inorganic sheet in the n = 1 (001)-orientation perovskites is less than 1nm.[57] Reducing dimensionality increases the separation of valence and conduction bands, and meanwhile, the bad gap becomes larger. For instance, the band gap of 3D perovskites $(CH_3NH_3)PbI_3$ ($MAPbI_3$) from 1.65eV[58] raises to 2.58eV[59] as the dimension reduces to 2D structure, which is $(C_6H_5(CH_2)_2NH_3)_2PbI_4$ (PEA_2PbI_4). Practically,

doi:10.6342/NTU201903018

quantum wells and layered perovskites properties are quite similar, and both of them characterize strong exciton binding energy and enhancement of luminescence relative to their 3D analogues.[60]

3.1 Excitons

The excited electrons and holes cannot be separated completely and have a Coulombic attraction, which form a status with electrostatically neutral quasiparticle, called exciton. Relating to free carriers, the excitons are stabilized by the exciton binding energy (E_b), which quantitative magnitude demonstrates the energy need to separate the Coulombic force between electrons and holes. Free carriers dominant in the 3D perovskites $(CH_3NH_3)PbI_3$, due to low exciton binding energy estimated at ca. 2 meV.[61] In contrast, the 2D lead-iodide perovskites have an exciton binding energy about ca. 300 meV, which E_b is stronger than 3D pervoskites' E_b.[57]

3.2 Determining the Band Gap (E_g) and Exciton Binding Energy (E_b)

At liquid helium temperature(4K), E_g and E_b can be directly determined from absorption spectra, which has an obvious stepped onset below their direct band gap (Figure 3.1 (a)),[62-63] and the E_b is determined by E_g – (excitonic peak energy), illustrated

doi:10.6342/NTU201903018

by Figure 3.1 (b). Generally, the optical band gaps of semiconductors are determined by Tauc plot method.[64] However, this method was developed for amorphous and electronically 3D materials which almost no excitonic effects,[58, 65] and hence, it is not suitable used for highly exciton bind energy materials such as group 14 layered perovskites.

(a) (b)

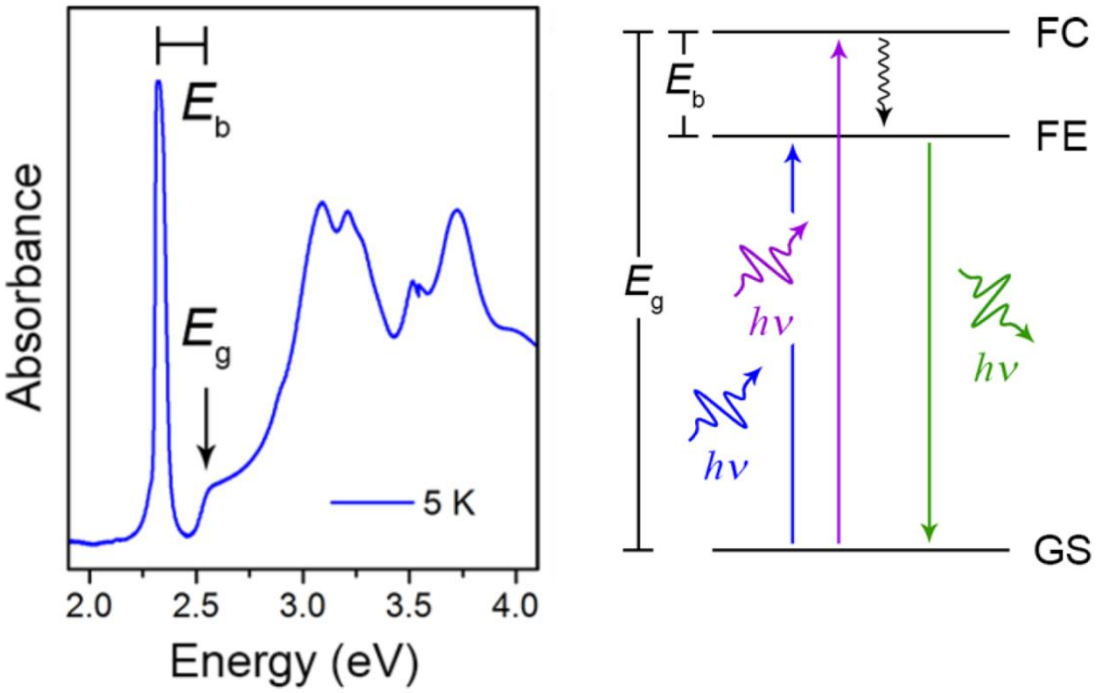

Figure 3.1 (a) Optical absorption spectrum of a 2D Pb−I perovskite (E_g = band-gap energy; E_b = exciton binding energy).[63] (b) Energy-level diagram of the typical excitonic and band-to-band transitions of 2D lead halide perovskites[62] (FC = free carriers state GS = ground state.; FE = free excitons state).

doi:10.6342/NTU201903018

3.3 Electronic Confinement Effects

For group 14 perovskites, 2D perovskites have stronger exciton binding energy compared to their 3D analogs, which is resulting from the combined effects of quantum and dielectric confinement. In spite of the difference between the true quantum-well systems and the layered perovskites, those two effects illustrate 2D perovskites' remarkably enhanced E_b. Quantum confinement (Figure 3.2) can increase the exciton binding energy such that the exciton binding energy of the 1s exciton is $\mathbf{E_b} = \left(\frac{\mathbf{2}}{\boldsymbol{a-1}}\right)^{\mathbf{2}} \mathbf{E_{b,3D}}$ where $\mathbf{E_b}$ is the exciton binding energy, $\mathbf{E_{b,3D}}$ is the exciton binding energy of bulk materials, and α is the dimensionality of system. In a bulk or non-confinement system, α is 3 and in a perfect 2D system α is 2, so we can get a corresponding exciton binding energy $\mathbf{E_{b,2D} = 4E_{b,3D}}$. Dielectric confinement is an electrostatic phenomenon that results as one material with a dielectric constant ε_1 is sandwiched between another material with a dielectric constant ε_2 ($\varepsilon_1 >> \varepsilon_2$). The electric field of medium material with high dielectric constant (ε_1), which is usually inorganic layers, penetrate to the outer material with low dielectric constant (ε_2), which is usually organic layer. Due to low dielectric constant of outer material, it decreases the screening of the hole−electron Coulomb interaction and lead to increase the exciton binding energy (Figure 3.3).[66]

doi:10.6342/NTU201903018

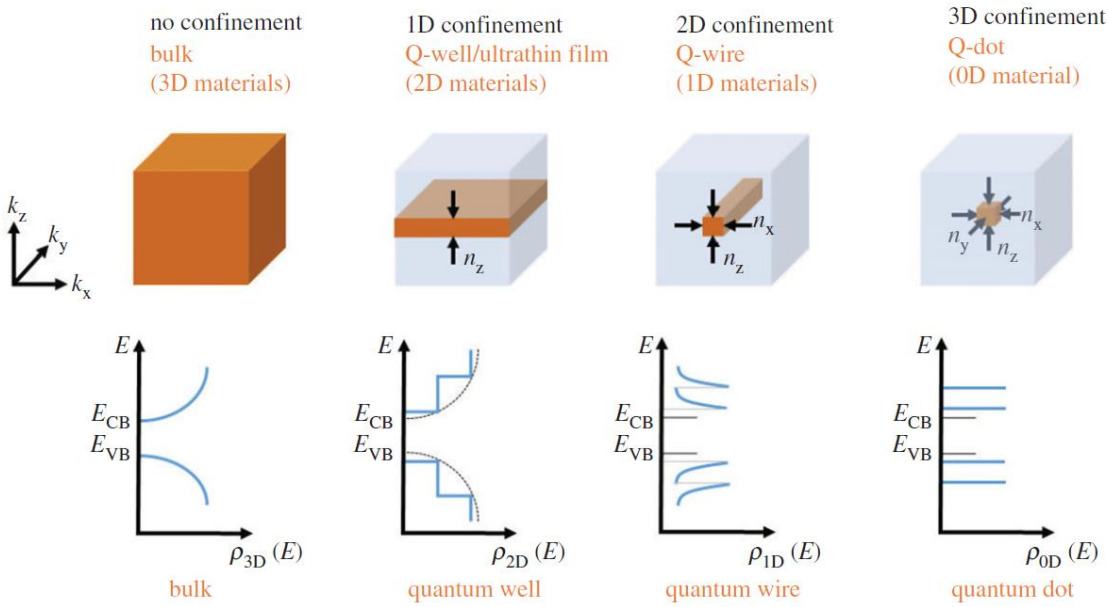

Figure 3.2 Schematic illustration of broken symmetry and functional form of the density of states in 1D, 2D and 3D confined materials.

doi:10.6342/NTU201903018

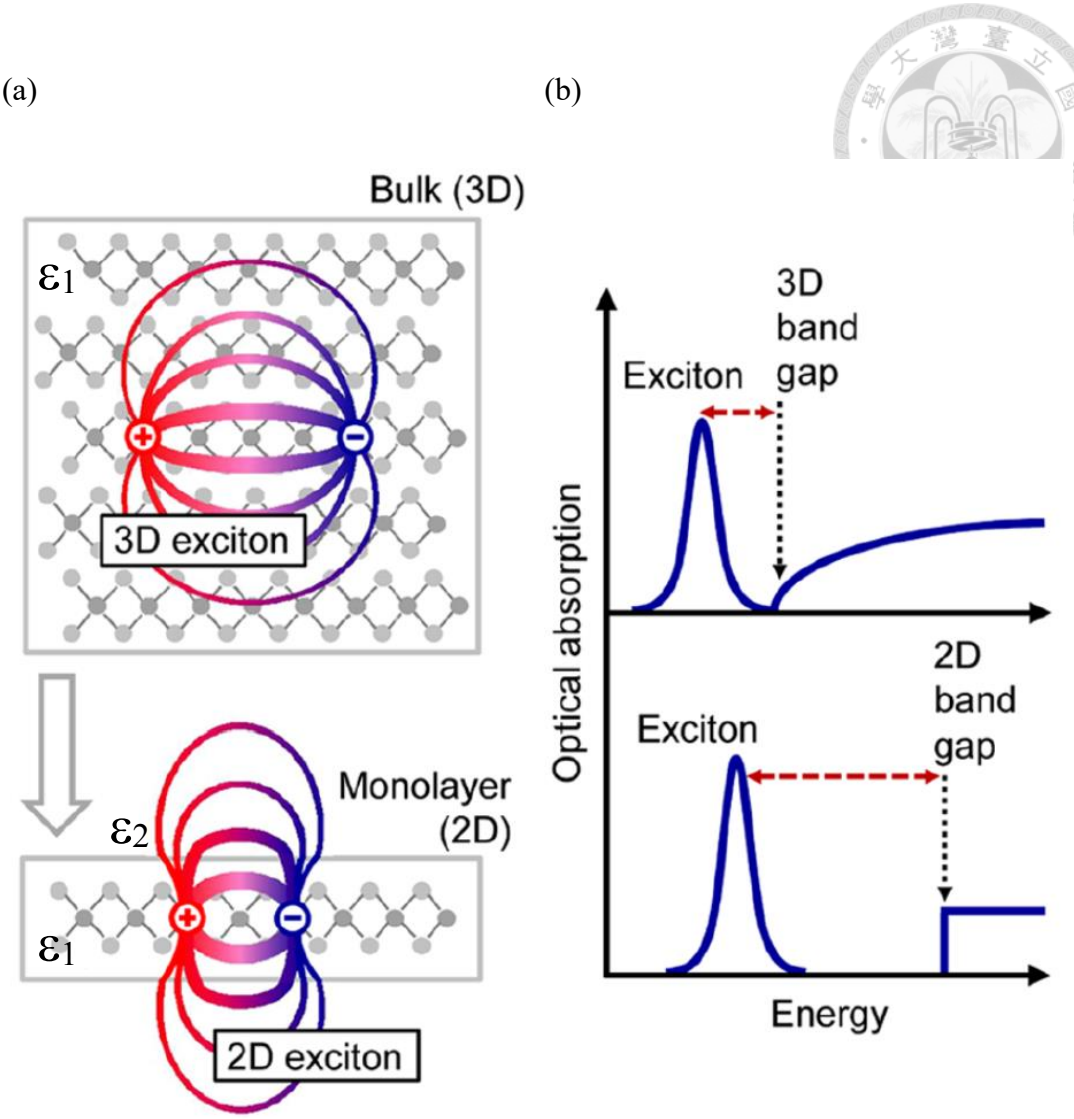

Fig 3.3 (a) Real-space representation of electrons and holes bound into excitons for the 3D bulk and 2D monolayer. ε_{3D}, ε_{2D} and ε_0 are indicated the dielectric constant of 3D material, 2D material, and vacuum, respectively (b) The transition from 3D to 2D is expected to lead to an increase of both the band gap and the exciton binding energy (indicated by the dashed red line).

doi:10.6342/NTU201903018

3.3.1 Tuning E_b through the Organic Layer

The dielectric constant (ε) of organic and inorganic layer mismatch may be decreased by involving polarizable groups in the organic layers. Ishihara et al. indicated the above impacts at their report. At n = 1 perovskites, which was synthesized by decylamine with ε ~ 2.44 and phenethylamine with ε ~ 3.32, respectively, they observed the E_b = 320 meV for $(C_{10}H_{21}NH_3)_2PbI_4$ and E_b = 220 meV for $(C_6H_5(CH_2)_2NH_3)_2PbI_4$ from absorption spectra.[59] Increasing ε of organic layer can enhance more screening effect, leading to lower exciton binding energy, E_b. Hence, with this strategy, Karunadasa et al. added iodoalkanes in the organic layers to increase ε of the organic layer and successfully synthesized $(IC_6)_2PbI_4$ and $(IC_6)_2PbI_4{\cdot}I_2$ (IC_6 = 6-iodohexan-1-aminium) layered perovskites with exciton binding energy 230 meV and 180 meV, respectively. Comparing to general 2D lead-iodide perovskites' E_b which value is usually over 300 meV, the E_b of $(IC_6)_2PbI_4$ and $(IC_6)_2PbI_4{\cdot}I_2$ are quite low.[63]

3.3.2 Tuning E_b through the Inorganic Layer

The composition of perovskites with different halides seem to influence the polarizability and then affect the E_b. For instance, the lead-iodide perovskites exhibit lower E_b values than lead-bromide perovskites since I^- has more delocalized electronics.[59, 67] In addition, pseudohalides also can affect the E_b. The thiocyanate (SCN^-) as the terminal

doi:10.6342/NTU201903018

ligands forming the layered perovskite $(CH_3NH_3)_2PbI_2(SCN)_2$ exhibits an E_b of 200 meV, which is lower than the n = 1 perovskite without polarizable groups organic layers.[68] Another route to reduce E_b is to increase the thickness of inorganic layers, which also reduces the band gap (E_g). The intermediate between n = 1 and n = ∞ shows intermediate properties. For example, the members of n = 1 perovskites, $(PEA)_2(MA)_{n-1}PbI_{3n+1}$, have E_g and E_b values of 2.58 eV and 220 meV, respectively, and n = 2 perovskites have corresponding values of 2.34 eV and 170 meV, respectively,[59] as well as n = 3 perovskites have further low corresponding values.[69] This tendency also applies to higher n values of perovskites and converges toward the n = ∞ perovskites.

doi:10.6342/NTU201903018

Chapter 4 Lead-Free and Low-Lead Perovskites

Lead is a toxic metal, whose widespread usage has given rise to serious environmental pollution and health problems. Lead can accumulate and it is extremely difficult to excrete outside the human body, causing irreversible health effects, and interfering with a number of body functions, including hematopoietic, hepatic, central nervous, and renal system. The toxicity of lead is a profound potential worry for commercialization. Though the lead perovskites solar cells have remarkable performance, their toxicity might be an obstruct for industrialization and is a serious concern for the public. In 2003, the European Union passed an Environmental Directive (Restriction of Hazardous Substances Directive 2002/95/EC, RoHS), which specifies the allowable weight ratio of a number of substances in electrical appliances, including lead (<1000ppm), cadmium (<100ppm), mercury (<1000ppm), polybrominated biphenyl (<1000ppm), and so on. Recently, World Health Organization (WHO) has considered Pb as one of the most toxic materials, which may affect human health and the environment, and is making rigorous policies to avoid usage of Pb. According to United State Environmental Protection Agency (U.S. EPA) policies, the maximum permissible amount Pb is 15 and 0.15 μg/L in water and air, respectively. Compared to the amount of lead (0.4 g) estimate in a 1 m^2 solar panel with 300 nm thick perovskite layer, U.S. EPA standards

doi:10.6342/NTU201903018

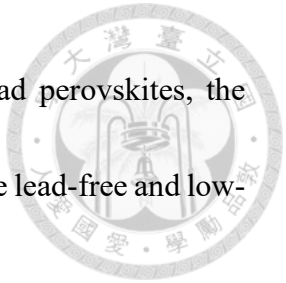

are quite low. Although their performance cannot compare with lead perovskites, the issues of lead toxicity have provided a strong motivation to develop the lead-free and low-lead perovskites.

4.1 Lead-Free Perovskite Materials

According to Goldschmidt tolerance factor and ionic size, some alternative metal cations are predicted to form perovskite structures, which may replace the lead perovskite's leading position in the future. Some divalent metals, including group 14 elements such as Sn^{2+} and Ge^{2+}, alkaline earth metal such as Be^{2+}, Mg^{2+}, Ca^{2+}, Sr^{2+}, and Ba^{2+}, transition metals such as V^{2+}, Mn^{2+}, Fe^{2+}, Co^{2+}, Ni^{2+}, Pd^{2+}, Cu^{2+}, Zn^{2+}, Cd^{2+}, and Hg^{2+}, lanthanides like Eu^{2+}, Tm^{2+}, and Yb^{2+}, and p-block elements like Ga^{2+} and In^{2+}, can form perovskites and be the alternatives of lead. Among those candidates, Sn^{2+} and Ge^{2+} are considered as two of most forward-looking alternatives.[70] Nevertheless, they still have some essential problems to be solved.

4.1.1 Tin (Sn)-Based Perovskites

As the most forward-looking candidates of lead alternative, Sn-based perovskites have been probed and defined as the first lead-free perovskite due to the similar ionic radii of Sn^{2+} (1.35 Å) and Pb^{2+} (1.49 Å).[71] Inspiringly, comparing to lead analogues, Sn-based perovskites exhibit lower band gap as well as higher charge carrier mobility of 10^2-

doi:10.6342/NTU201903018

10^3 $cm^2/V{\cdot}s$.[14] In addition, the major 3D Sn-based perovskites show E_b value ca. 2-50 meV, which is similar to lead analogues.[72] Therefore, Sn-based perovskites have other promising optoelectronic properties like narrow optical band gap, wide absorption range from ultraviolet (UV) to near-infrared (NIR), good electrical conductivity, long diffusion length, as well as excellent electron mobility. Nevertheless, Sn^{2+} suffers from its extreme instability. The oxidation Sn^{2+} to Sn^{4+} is caused by its inherent propensity, which generates high defect density and surface trap. With this serious disadvantage, currently, tin-base perovskites performance is unable to compare with lead-based perovskites.

As the above illustrates that Sn^{2+} prefer to oxidation, some studies add extra Sn^{2+} precursor such as SnI_2,[73] $SnCl_2$,[74] and SnF_2[75] to precursor solution as a compensator to fill the vacancies. Among these tin(II) halides, SnF_2 is the most widely used. A number of studies indicate that SnF_2 can effectively suppress and reduce the rate of Sn^{2+} oxidation.[76] In addition, some additives also have the similar features as SnF_2 like hydrazine (N_2H_4)[75, 77] and hypophosphorous acid (H_3PO_2),[78] which act like reducing agents. To improve the Sn-based perovskite stability, reduced dimensionality is also an alternative. According to Edward H. Sargent et al. research, different ammonium salts have different desorption energy which significantly influences perovskite stability. For example, comparing $MAPbI_3$ (MA^+= $CH_3NH_3^+$) with PEA_2PbI_4 (PEA^+ = C_6H_5-$CH_2NH_3^+$), the desorption energy of ammonium salts separates from perovskite surface

doi:10.6342/NTU201903018

to air is 2.15 eV and 2.51 eV, respectively. The difference between them is 0.36 eV due to the van der Waals force between the different ammonium salts. At high humidity environment, the desorption rate of PEA^+ is six orders slower than MA^+, and the degradation rate of MA^+ is 1000 times faster than PEA^+. Therefore, using high desorption energy, ammonium salt can stabilize the perovskite structure. That is, compared with the three-dimensional perovskite structure composed of small ammonium salts (ex. MA^+), larger ammonium salt (ex. PEA^+) has stronger van der Waals force and forms two or lower dimensional perovskite with better stability.[79] In summary, though there are many methods to improve Sn-based perovskites stability, those methods also have some disadvantages. The usage of SnF_2 compensates the tin-based perovskite Sn^{2+} vacancies, but the complete mechanism of this additive and the role of halides (F and I) arrangement, whose ionic radius is too different, are still unclear. Besides, hydrazine is a toxin, which can affect human health and the environment; hypophosphorous acid suppresses Sn^{2+} oxidation but reduce the performance. In addition, low dimensional Sn-base perovskites haven't been explored more to find ways to stabilize the Sn perovskite longer.

4.1.2 Germanium (Ge)-Based Perovskites

Germanium (Ge), which is also a family of group 14, can form perovskite structure and doesn't violate the Goldschmidt tolerance factor. Ge-based perovskites ($AGeX_3$) own

doi:10.6342/NTU201903018

the similar optical and electric properties as its analogues, lead and tin, due to its divalent nature.[80] Both theoretical[81] and experimental[15] studies have indicated that the band gap of Ge-based perovskites depend on its halide ions, and this property is similar to its analogues. For example, in case of $CsGeI_3$, $CsGeBr_3$, and $CsGeCl_3$, their E_g varies from 1.6 eV to 2.3 eV and to 3.2 eV, respectively. However, there are not much study to develop Ge-based perovskite, but the similar properties of tin- and lead-based perovskites make it a promising alternative to Pb perovskites.

4.1.3 Lead-Free Binary Metal Halide Perovskites

Combining two divalent metals simultaneously may improve the performance and stability. Sn-Ge bimetallic compositions have exhibited promising performance and stability at field of solar cell. This year, Nitin P. Padture and co-worker reported a perovskite solar cell with formula $CsSn_{0.5}Ge_{0.5}I_3$ having power conversion efficiency (PCE) of 7% and extreme high air stability under continuous light illumination over 100 hours with more than 80% of original efficiency and without encapsulation. Due to surface native oxidation, the internal Sn-Ge perovskites are completely protected and exhibit significant high stability and efficiency.[82]

doi:10.6342/NTU201903018

Chapter 5 Experiment

5.1 Experiment Motivation

Due to the threat from lead toxicity, lead-free perovskites have rapidly developed in these years. Among those candidates above, tin (Sn) is considered to be the most promising alternative. However, the rapid oxidation form Sn^{2+} to Sn^{4+} is a difficult issue. Although a number of studies utilize many methods to eliminate Sn^{4+} generation, such as adding extra Sn^{2+} precursor like SnI_2, $SnCl_2$, and SnF_2 as compensators, using reducing agents like hydrazine (N_2H_4) and hypophosphorous acid (H_3PO_2), reducing dimension from 3D to 2D to stabilize, or combining germanium (Ge) to form Sn-Ge perovskites, most of them didn't quantify the ratio of Sn^{4+} to Sn^{2+}. Additionally, most of the research about tin-based perovskites focus on the field of solar cell, but there is no special attention in the luminescence prosperity. Here, we want to summarize some previous studies about tin-based perovskites luminescence. Jellicoe et al. studied lead-free cesium tin halide perovskite nanocrystals and provided evidence of their spectral tunability through both quantum confinement effects and control of the halide composition. The resulting $CsSnX_3$ nanocrystals exhibited a relatively low photoluminescence quantum yield (PLQY) of <0.14% and broad full width at half maximum (FWHM; ≥100 nm).[83] In addition, by replacing Cs^+ cations with butylammonium (BA) or octylammonium (OA), Tisdale and

doi:10.6342/NTU201903018

co-workers synthesized a 2D perovskite nanoplates with one-layered (n = 1) L_2SnI_4 and double-layered (n = 2) $L_2[FASnI_3]SnI_4$ (L: BA, OA) structure; for these nanoplates, the PLQY was increased to 0.5 % for L_2SnI_4 (n = 1) and 2.6 % for $L_2[FASnI_3]SnI_4$ (n = 2).[84] Last year, our group successfully developed PEA_2SnX_4 (PEA = $C_6H_5(CH_2)_2NH_3$, X = Br, I) by replacing BA^+ with phenylethylammonium (PEA). PEA_2SnX_4 is accompanied with strongly coupled layered structures, which shows an emission at a wavelength of 640 nm, with high quantum yield of 6.40 ± 0.14 % and full width at half maximum (FWHM) as small as 36 nm.[85] Most recently, our group used Thiopheneethylammonium (TEA), which have stronger coupling force and exciton binding energy than PEA, as A-site cation and got incredible high PLQY of up to 21 % with the assistance pentanoic acid.[86] Furthermore, some studies of perovskites have focused on pseudohalide additive such as SCN^-,[87] tetrafluoroborate[88-89] and hexafluorophosphate.[90] However, these studies usually focus on lead-based perovskites, and as far as our knowledge is concerned, there is only one report on the addition of pseudohalide to tin-based perovskites.[91] According to previous studies about tin perovskites luminescence, most of high luminescence tin perovskites are based on two-dimensional materials. Hence, we want to combine tin-based perovskites with pseudohalides to elucidate the performance and stability of tin-based perovskites after adding various pseudohalide, and attempt to explain this phenomenon.

doi:10.6342/NTU201903018

5.2 Experimental Section

5.2.1 Chemical

Chemicals listed below are commercially available and used without further purification. Tin iodide (SnI_2, Sigma-Aldrich, 99.999 %), Hydroiodic acid (HI, Acros, 57 wt.% in water), 2-Phenylethylamine (PEA, TCI, >98 %), 2-Thiopheneethylamine (TEA, TCI, >98 %), Tetrabutylammonium cyanate (TBAOCN, Sigma-Aldrich, technical), Ammonium thiocyanate (NH_4SCN, Sigma-Aldrich, 99.99 % trace metals basis), Ammonium iodide (NH_4I, Sigma-Aldrich, ≥99 %), Tetrabutylammonium iodide (TBAI, Sigma-Aldrich, 98 %), Ammonium hexafluorophosphate (NH_4PF_6, Sigma-Aldrich, ≥99.98 %), Ammonium tetrafluoroborate (NH_4BF_4, Sigma-Aldrich, ≥99.99 %), Potassium selenocyanate (KSeCN, Sigma-Aldrich, ≥99 %), Potassium iodide (KI, Sigma-Aldrich, ≥99 %), Toluene (Sigma-Aldrich, anhydrous, 99.8 %), Dimethylformamide (Sigma-Aldrich, anhydrous, 99.8 %).

5.2.2 Synthesis methods

Nanoplates synthesis: syntheses of TEA_2SnI_4 nanoplates follow a facile procedure. The starting precursor at concentration of 1 M was prepared by dissolving SnI_2 (372.5 mg, 1 mmol) and TEAI (510.2 mg, 2 mmol) in 1 mL DMF. 8 μL precursor solution was then

doi:10.6342/NTU201903018

added to 4 mL of antisolvent, followed by stirring for 1 minute. The solution was centrifuged at 3500 rpm for 40 seconds, and then supernatant and were collected for further characterization. All synthetic steps were operated under inert atmosphere in a glovebox.

Preparation of NH_4SCN solution in DMF: the NH_4SCN solution at concentration of 1 M was prepared by dissolving NH_4SCN (76.1 mg, 1 mmol) in 1 mL DMF.

Preparation of NH_4SCN saturation solution in toluene: the amount NH_4SCN added in toluene and the heterogeneous mixture was stirred at room temperature for 30 minutes. mixture. The remaining salt was removed from solution by either centrifugation followed by decanting or by using a PTFE syringe filter.

Pre-treatment method to synthesize nanoplates: using TEA_2SnI_4 with 7% NH_4SCN additive as an example, we added extra 70 μL 1 M NH_4SCN solution in the 1 mL starting nanoplates precursor at concentration of 1 M. 8 μL precursor solution was then added to 4 mL of antisolvent, followed by stirring for 1 minute. The solution was centrifuged at 3500 rpm for 40 seconds, and then supernatant and were collected for further characterization.

doi:10.6342/NTU201903018

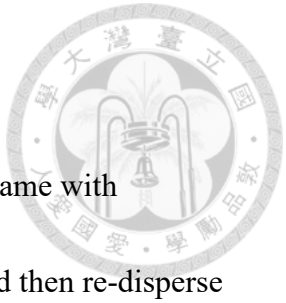

Post-treatment method to synthesize nanoplates: initial steps are the same with *Nanoplates synthesis.* After centrifuging, we removed supernatant and then re-disperse nanoplates in toluene of NH_4SCN saturation solution, and next, stirred for 30 minutes. The final solution was centrifuged at 3500 rpm for 40 seconds, and then supernatant and were collected for further characterization.

Post-treatment method to synthesize nanoplates: initial steps are the same with *Nanoplates synthesis.* after we obtained prepared perovskites, we added extra 2μL of 1M DMF NH_4SCN solution in and stirred further 5 minutes. The final solution was centrifuged at 3500 rpm for 40 seconds, and then supernatant and were collected for further characterization.

doi:10.6342/NTU201903018

Chapter 6 Results and Discussions

In this experiment, the amine salt of TEA^+ was selected to synthesize a single layer of TEA_2SnI_4 nanoplate. After we injected precursor solution in toluene, the product was rapidly precipitated and dispersed in this poor solvent. Besides, we can observe the PLQY value of TEA_2SnI_4 is 5.8 %, which is higher than our last report of PEA_2SnI_4 (before pentanoic acid assistance PLQY = 2.7 ± 0.2 %).[85] Though this value is quite high at tin-based perovskites, it cannot compare to lead-based perovskites. Low air stability is a big issue to tin-based perovskites, and we want to follow our last few reports' idea of adding certain additives to control tin-iodide perovskite nanoplates nucleation process. By using this strategy, we intend to suppress Sn^{4+} generation and obtain tin-iodide perovskite nanoplates with higher stability. To improve air stability, Seok et al. reported that mixed halide perovskites $CH_3NH_3PbI_{3-x}Br_x$ have higher stability when 10 – 15 mol % I^- was substituted by Br^-. The enhanced stability was attributed to the stronger interaction between Br^- and $CH_3NH_3^+$.[92] Hence, we considered pseudohalide salts, such as cyanate, thiocyanate, selenocyanate, tetrafluoroborate, and hexafluorophosphate, have similar property, and are good candidates as additives. To confirm the counter cation of pseudohalide influence, we added extra 5% potassium iodide (KI), ammonium iodide (NH_4I), and tetrabutylammonium iodide (TBAI) to TEA_2SnI_4 precursor solution and

doi:10.6342/NTU201903018

synthesized TEA_2SnI_4 nanoplate. Figure 4.1 (a)-(c) are the absorption and photoluminescence of the TEA_2SnI_4 nanoplate with corresponding additives. There is no peak shift and intensity variation, that is, those counter cations don't affect the formation and structure of TEA_2SnI_4 nanoplate. The PLQY of the different proportions of pseudohalides is shown in Table 2.1.

doi:10.6342/NTU201903018

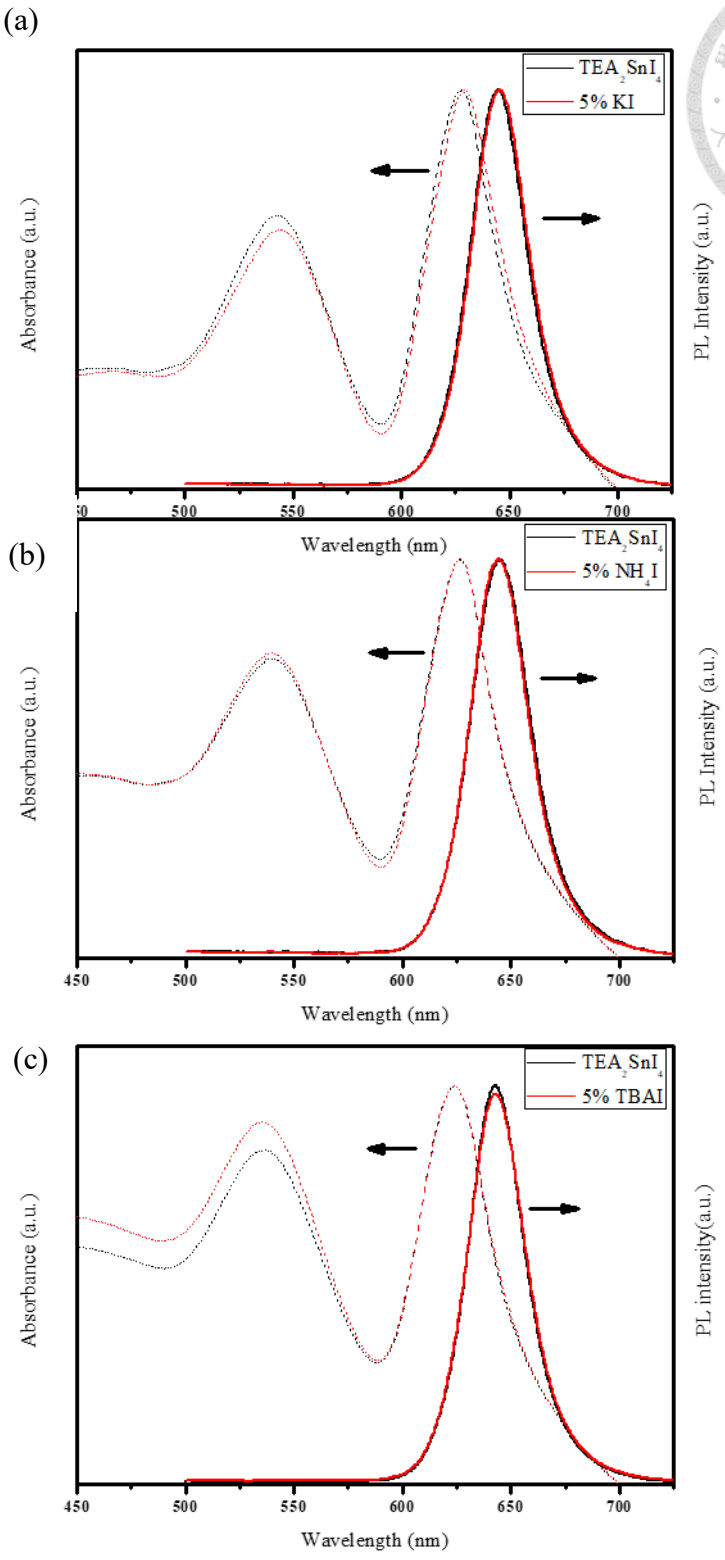

Figure 4.1 Absorption and photoluminescence of the TEA_2SnI_4 nanoplate with (a) 5 % KI (b) 5 % NH_4I (c) 5 % TBAI

doi:10.6342/NTU201903018

Table 2.1 The summary PLQY of different proportions of pseudohalide additives.

Pseudohalide / PLQY(%) / Adding amount	NH_4BF_4	KPF_6	KSeCN	NH_4SCN	TBAOCN
0%	5.8 ± 0.2	5.8 ± 0.2	5.8 ± 0.2	5.8 ± 0.2	5.8 ± 0.2
1%	4.8± 0.2	4.5 ± 0.1	5.0 ± 0.2	8.7 ± 0.5	7.2 ± 0.6
3%	4.5 ± 0.1	4.2 ± 0.3	4.5 ± 0.3	12.6 ± 1.2	8.5 ± 0.9
5%	4.1 ± 0.1	3.9 ± 0.2	3.8 ± 0.3	15.3 ± 2.0	10.5 ± 1.3
7%				19.5 ± 2.3	12.5 ± 1.8
9%				16..4 ± 1.9	8.9 ± 1.5

doi:10.6342/NTU201903018

According to Table 1.1, the PLQY of the TEA_2SnI_4 nanoplate is highly correlated with the structure of the pseudohalide additive, and there is a trend to follow. Linear structure of pseudohalide can improve PLQY of TEA_2SnI_4 nanoplate, but the result of $SeCN^-$ cannot follow this trend. $SeCN^-$ seems to gradually oxidize Sn^{2+} to Sn^{4+} in an inert environment. We observed the color of precursor changes from light yellow to dark red after added $SeCN^-$ to TEA_2SnI_4 precursor solution. According to other research,[91] this dark red represents dead precursor which exists too much Sn^{4+} ions. Among those pseudohalide additives, thiocyanate (SCN^-) and cyanate (OCN^-) can enhance PLQY of TEA_2SnI_4 nanoplate, and such PLQY can increase to 22 % with the assistance of SCN^-.

Figure 4.2 (a) shows X-ray diffraction (XRD) patterns of tin-iodide perovskite nanoplates with various concentrations of NH_4CSN in the perovskite precursors: 0 %, 7 %, and 20 %. Figure 4.2 (b) shows XRD patterns from tin-iodide perovskite nanoplates with different linear pseudohalides at the proportion 7 %. Interestingly, the peak positions of the (002), (004), and (006) planes of TEA_2SnI_4 do not change as the amount of NH_4SCN increases and the same occurs for other linear pseudohalides.

doi:10.6342/NTU201903018

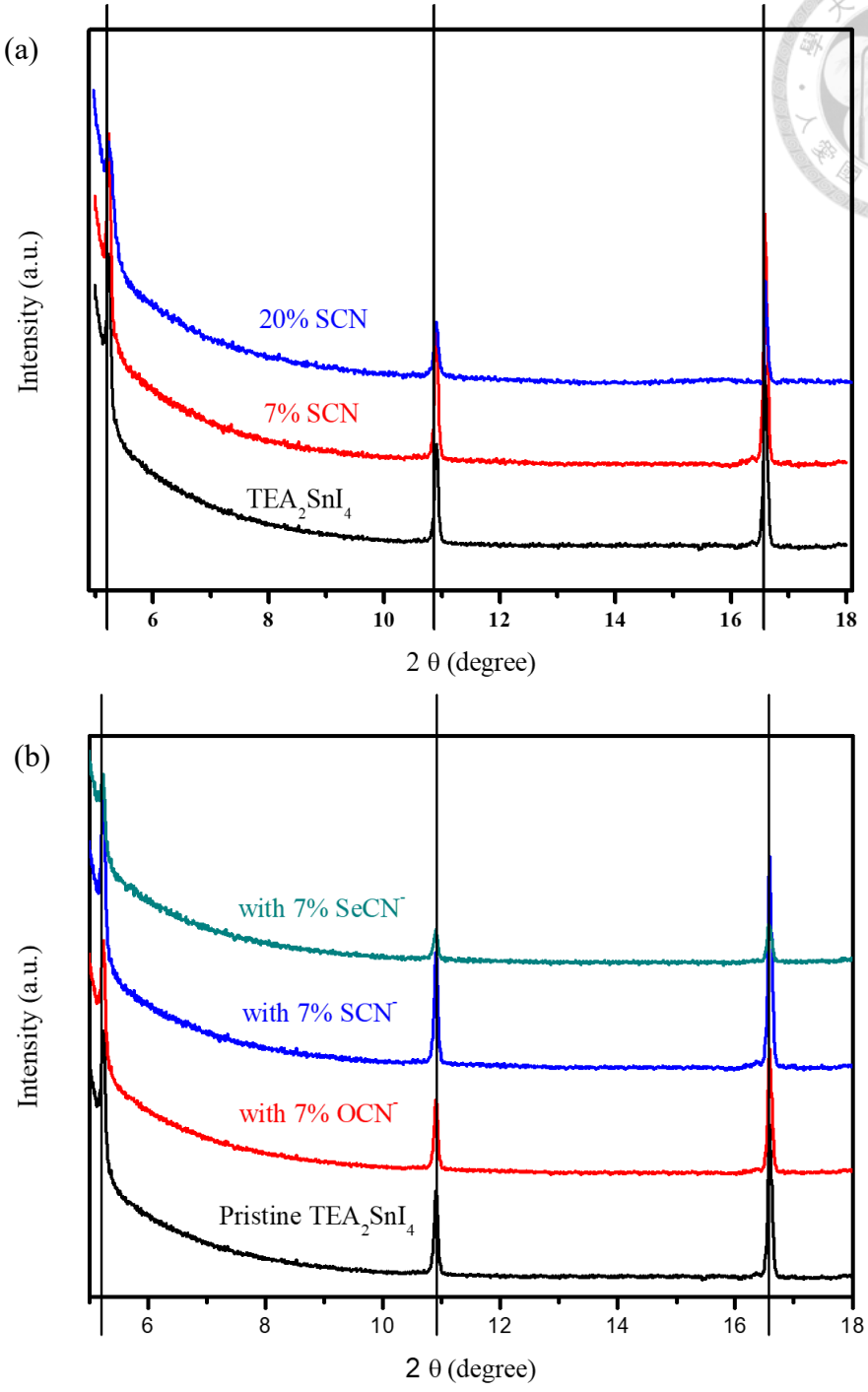

Figure 4.2 XRD pattern of (a) pristine TEA_2SnI_4 with 0 %, 7 %, and 20 % SCN^- (b) pristine TEA_2SnI_4 with 7 % OCN^-, with 7 % SCN^-, and with 7 % $SeCN^-$, respectively.

doi:10.6342/NTU201903018

Practically, the radius of I^- ion, OCN^- ion, SCN^- ion, and $SeCN^-$ are 0.21 nm,[93] 0.24 nm,[94] 0.25 nm,[93] and 0.27 nm[93] respectively. The differences radius should cause different d spacing from XRD pattern. If the linear pseudohalide ions substituted all Z axial sites of the final 2D tin perovskite, the shift in the XRD peak position of the (002), (004), and (006) plane should be observed. However, there is no shift of the diffraction peak in XRD results, so we suspect that most SCN^- ions do not remain in the tin-iodide perovskite structure. The following will explain and analyze about SCN^- ion additive because the highest PLQY observed.

We hypothesize that the presence of SCN^- ion can be confirmed by X-Ray photoelectric spectroscopy (XPS). Since TEA_2SnI_4 has a lot of sulfur element provided by 2-thiophene-ethylammonium, we used PEA_2SnI_4 with 7% NH_4SCN additive for our XPS analysis. As shown in Figure 4.3 (d), the XPS spectra of final tin-iodide perovskite nanoplates (PEA_2SnI_4) with 7 % NH_4SCN additive in the precursor measured by an in-house XPS does not show any evidence of sulfur. This result coincides with others. Since the excitation photon energy of in-house XPS is not adjustable, we use synchrotron radiation XPS to measure. The high excitation photon energy will make the electron kinetic energy also high, and the electronic signal of the internal material will be detected. The detection sensitivity of the sulfur signal region is very poor. If the probing depth is too deep, it will cause too much noise and the signal-to-noise ratio is too low. We used

doi:10.6342/NTU201903018

750 eV (Figure 4.4 (a)-(d)) and 260 eV (Figure 4.4 (e), (f)) excitation photon energy. As expected, the XPS spectrum did not have any identifiable sulfur signal as photon energy at 750 eV. Conversely, as photon energy at 260 eV, the XPS spectrum showed a trace of S signal. The XPS spectra (Figure 4.4 (f)) of final tin-iodide perovskite nanoplates (PEA_2SnI_4) with 7 % NH_4SCN in the precursor show the evidence of the sulfur presence in tin-iodide perovskite nanoplates.

doi:10.6342/NTU201903018

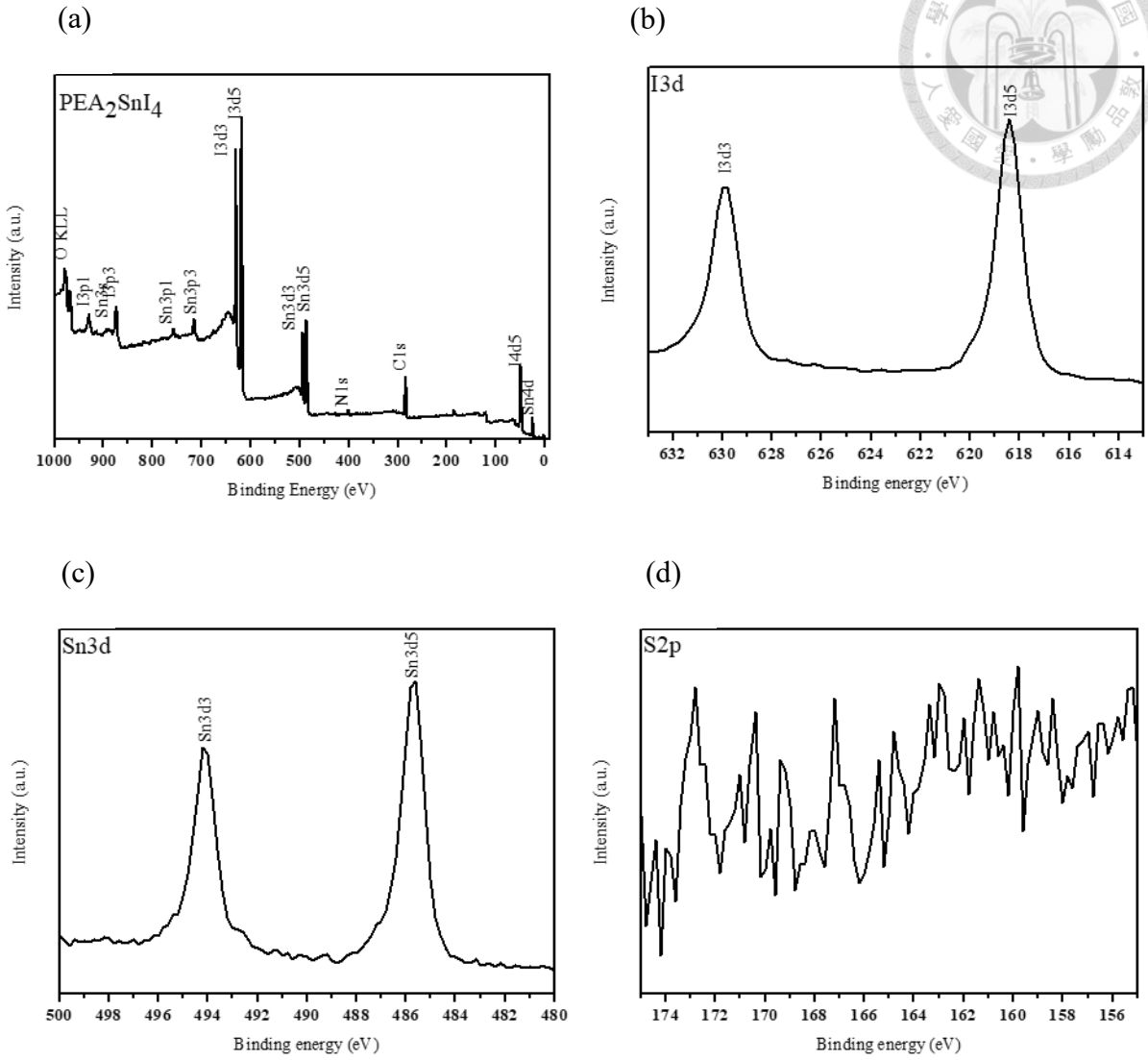

Figure 4.3 XPS spectra of PEA_2SnI_4 for (a) survey scan and high-resolution XPS spectra of (b) I 3d, (c) Sn 3d, and (d) S 2p.

doi:10.6342/NTU201903018

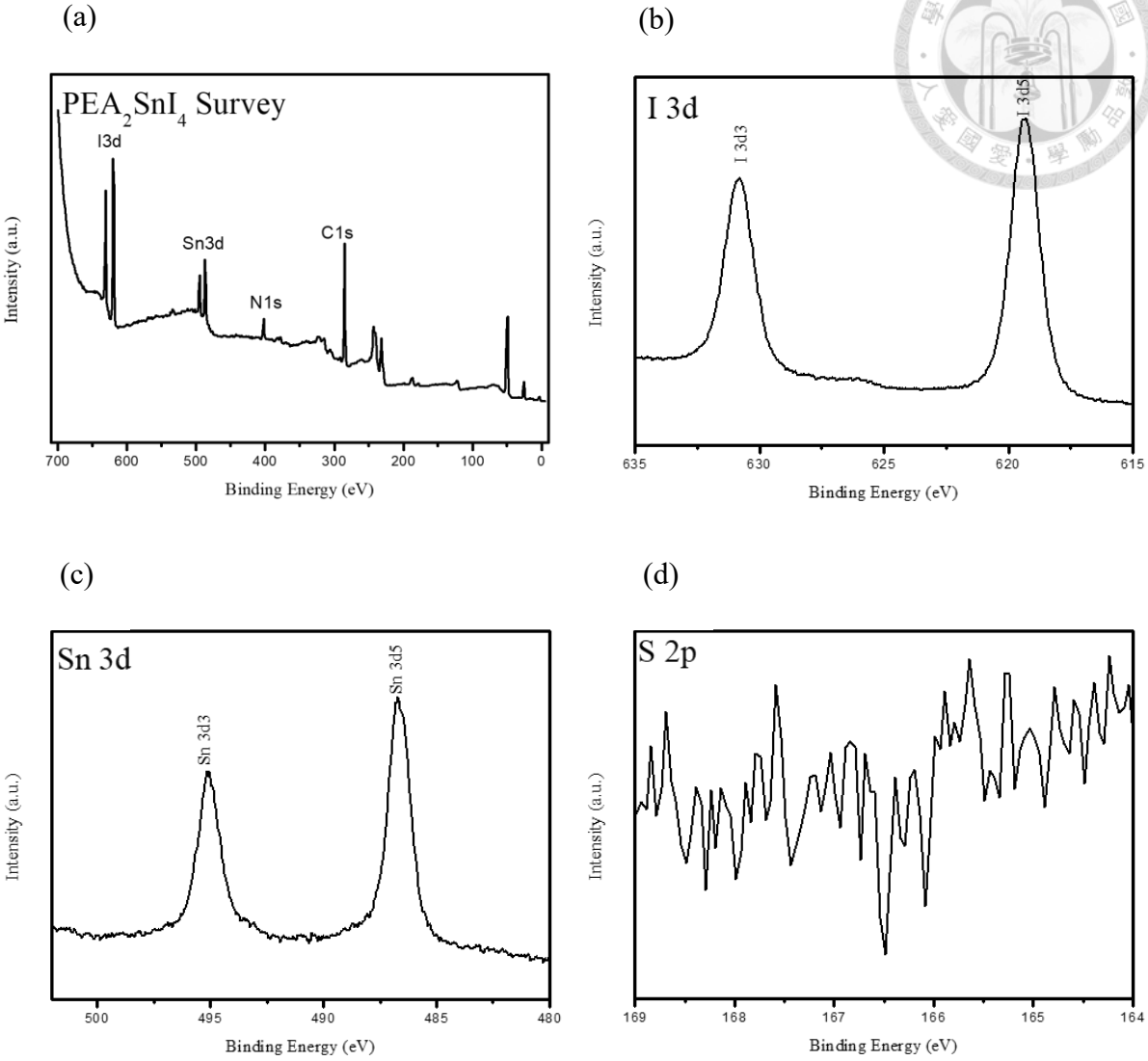

Figure 4.4 Synchrotron XPS spectra of PEA_2SnI_4 as photon energy is 750eV for (a) survey scan and high-resolution XPS spectra of (b) I 3d, (c) Sn 3d, and (d) S 2p.

doi:10.6342/NTU201903018

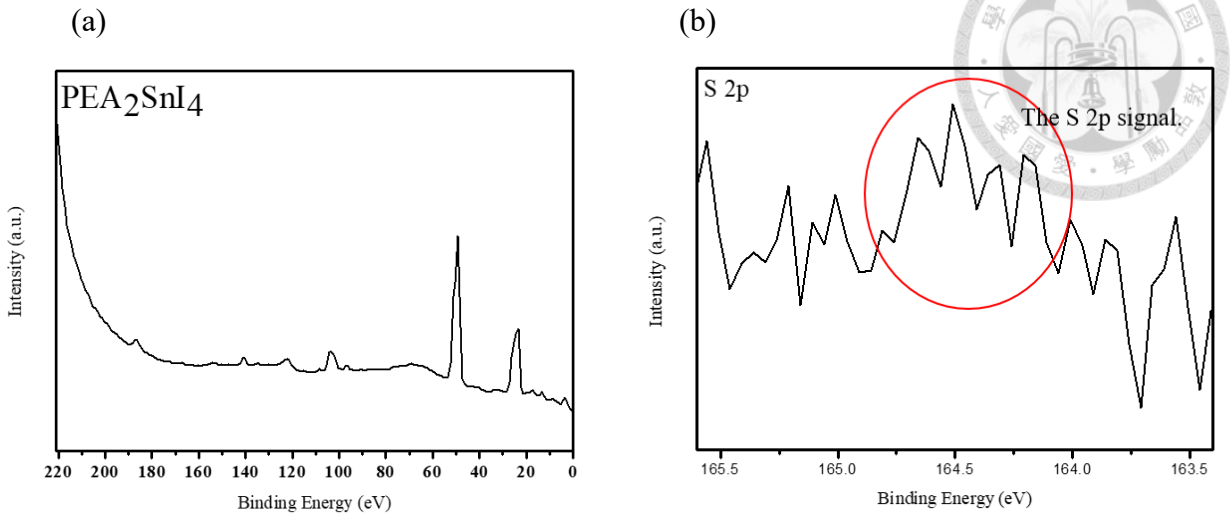

Figure 4.5 Synchrotron XPS spectra of PEA_2SnI_4 as photon energy is 260 eV for (e) survey scan and high-resolution XPS spectra of (f) S 2p.

doi:10.6342/NTU201903018

To confirm whether or not a trace amount of SCN^- ion remains on the surface of final tin-iodide perovskite nanoplates, TEA_2SnI_4 with 7% NH_4SCN additive in the precursors produce tin-iodide perovskite nanoplates product is measured by time-of-flight secondary ion mass spectrometry (ToF-SIMS) with a detection limit of as low as parts per billion (ppb). The TOF-SIMS imaging and depth profiling were utilized to confirm whether the SCN^- ion remain at the surface of tin-iodide perovskite nanoplates or not. Figure 4.6 and Figure 4.7 show the intensity mapping of the Sn, TEA, I, SCN, and total fragments signal, respectively. From ToF-SIMS mapping images (Figure 4.6 & Figure 4.7), signals of Sn fragments, TEA fragments, I fragments, and SCN fragments are overlap and all of these signals have strong contrast with substrate. It reveals that SCN^- indeed coordinate on the tin-iodide perovskite nanoplates. The ToF-SIMS depth profiles shown in Figure 4.8 indicate that the average SCN^- concentration in a final perovskite is very low, below the detection limit of XPS. Therefore, only a trace amount of SCN^- ions remains on the surface of tin-iodide perovskite nanoplates, which are not expected to cause detectable effects on the structural and optical properties of the tin-iodide perovskite nanoplates.

doi:10.6342/NTU201903018

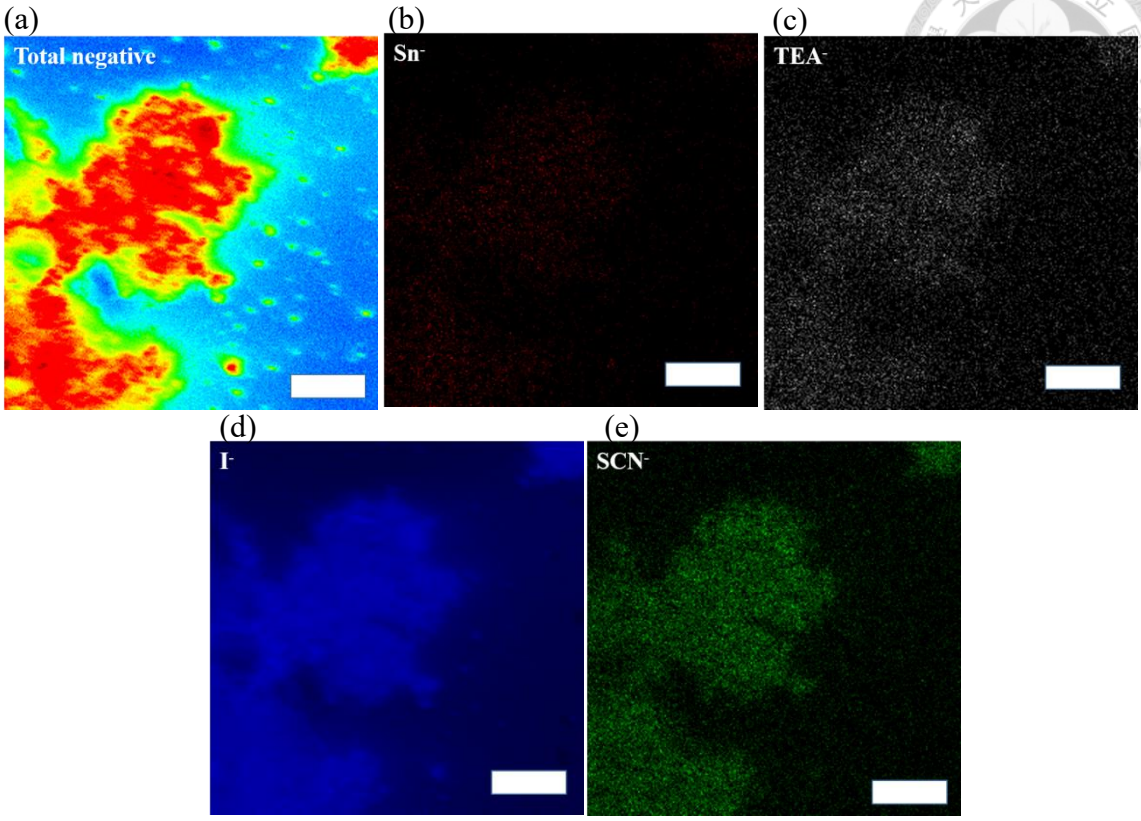

Figure 4.6 Negative signals of ToF-SIMS imaging (50 × 50 μm^2) of the TEA_2SnI_4 with 7% NH_4SCN additive. (a) Total$^-$, (b) Sn^-, (c) TEA^-, (d) I^-, and (e) SCN^-, respectively.

doi:10.6342/NTU201903018

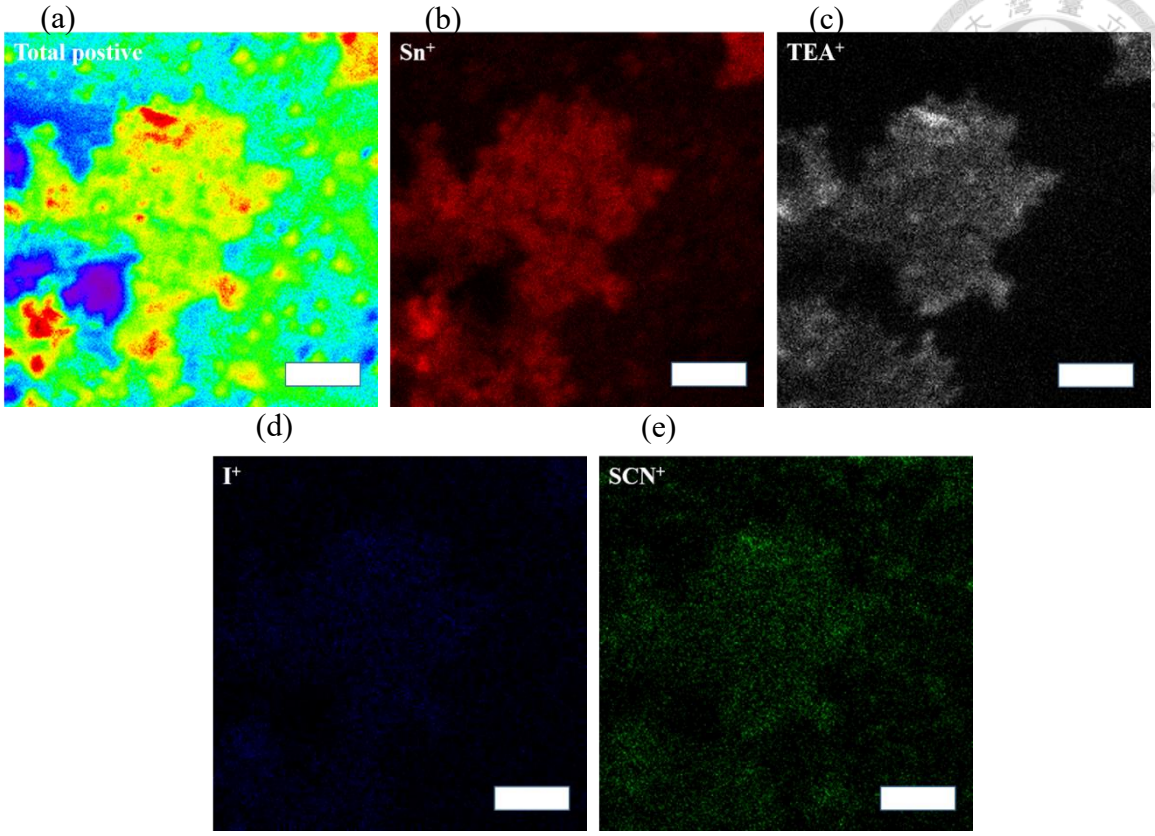

Figure 4.7 Positive signals of ToF-SIMS imaging (50 × 50 μm^2) of the TEA_2SnI_4 with 7% NH_4SCN additive. (a) Total$^+$, (b) Sn^+, (c) TEA^+, (d) I^+, and (e) SCN^+, respectively

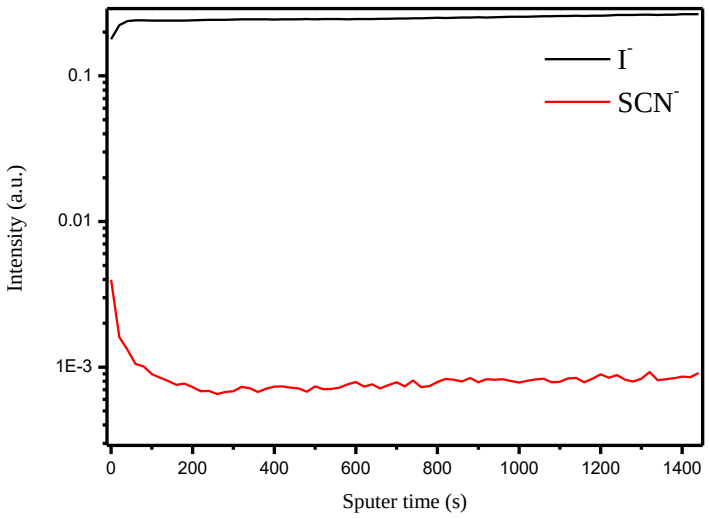

Figure 4.8 ToF-SIMS depth profiles of the thin films of TEA_2SnI_4 with 7 % NH_4SCN additive.

doi:10.6342/NTU201903018

Consolidating the above conclusions, XRD patterns describe that the d spacing of the tin-iodide perovskite nanoplates added with 7% NH_4SCN has not changed, synchrotron radiation X-Ray photoelectric spectroscopy and ToF-SIMS mapping images indicate that these is still a trace amount of SCN^- ions coordination on the tin-iodide perovskite nanoplates, and the ToF-SIMS depth profiles elaborate that SCN^- ions indeed incorporate with the surface of tin-iodide perovskite nanoplates. Combining these evidences, we can predict that TEA_2SnI_4 / $TEA_2SnI_{4-x}SCN_x$ is a core-shell like structure and this structure can intuitively illustrate the excellent air stability of our tin-iodide perovskite nanoplates.

Considering the core-shell like structure, something must have happened in the precursor solution just like Seok et al. proved PbI_2(DMSO) complex existence in the precursor solution leading to high quality perovskites.[95] We suspected that SCN^- can form complex with SnI_2, which can be confirmed by NMR. In precursor solution, SCN^- ions coordinate with tin(II) iodide, forming SnI_2-SCN complex, which has a significant upfield shift from -396 ppm to -432 ppm at ^{119}Sn NMR spectroscopy (Figure 4.7 (b)) and downfield shift from 130.5 ppm. to 134.3 ppm at ^{13}C NMR spectroscopy (Figure 4.7 (a)). This obvious shift was exhilarating and was a strong evidence to prove presence of SnI_2-SCN complex. Additionally, we considered the growth mechanism of TEA_2SnI_4 / $TEA_2SnI_{4-x}SCN_x$ is similar to the study of Seok et al.

doi:10.6342/NTU201903018

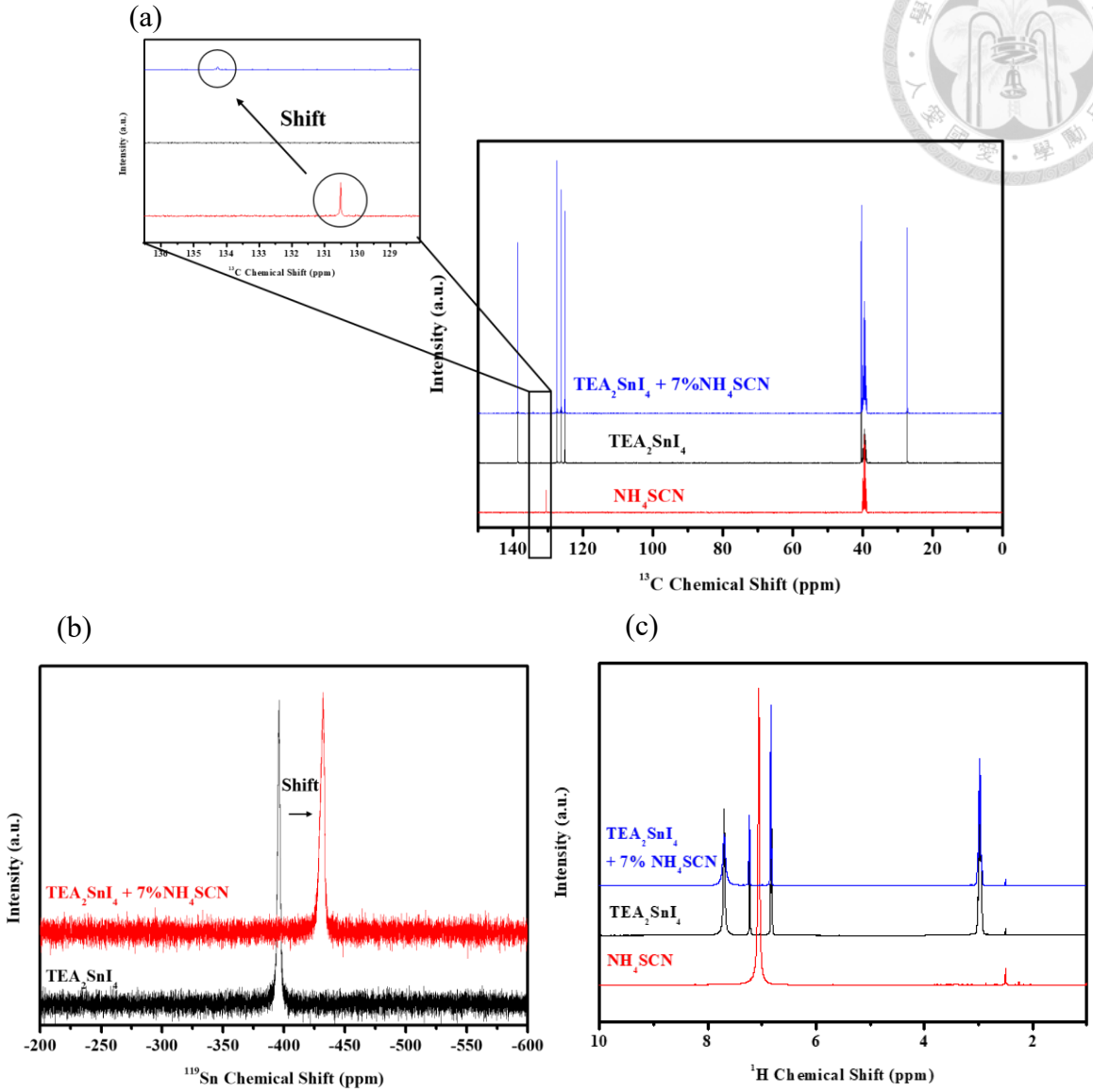

Figure 4.9 (a) ^{13}C NMR, (b) ^{119}Sn NMR, and (c) ^{1}H NMR of NH_4SCN, TEA_2SnI_4 and TEA_2SnI_4 with 7% NH_4SCN additive, respectively. All of these samples were prepared in solution in DMSO-d_7.

doi:10.6342/NTU201903018

Hence, we demonstrated a growth mechanism. First, $TEA_2SnI_{4-x}SCN_x$ forms on the surface of the TEA_2SnI_4, which results in a TEA_2SnI_4 / $TEA_2SnI_{4-x}SCN_x$ core / shell like structures. As expected from the conversion of SnI_2-SCN complex to TEA_2SnI_4 / $TEA_2SnI_{4-x}SCN_x$, the coordination of SCN^- ion with SnI_2 can't be easily replaced by external iodide ions because of strong S-Sn bond. Second, surrounding iodide ions slowly replace the SCN^- ion layer by layer. After the surrounding iodide ions exchange has ended, SCN^- ions can only coordinate on the surface of the surface tin-iodide perovskite nanoplates. Finally, it forms a TEA_2SnI_4 / $TEA_2SnI_{4-x}SCN_x$ core / shell like structures.

Due to significant enhancement in PLQY of tin-iodide perovskite nanoplates added with 7% NH_4SCN, we have a hypothesis that as long as the outermost tin-iodide perovskite nanoplates layer is bonded by SCN^- ions, the PLQY will increase. Therefore, we refer to the method of the Alivisatos et al. group. Alivisatos et al. synthesized trap-free $CsPbBr_3$ quantum dots assisted by SCN^-.[87] Comparing pre-treatment with post-treatment process, they observed that post-treatment process got near 100% photo luminance quantum yield (PLQY) and better stability because of the quantum dots surface traps were passivated by SCN^-. Here, we compared the pre-treatment and post-treatment process in Table2.2. The tin-iodide perovskite nanoplates synthesized in the two methods has a significant improvement in the light-emitting performance. The benefits of post-treatment process are not as good as the benefits of pre-treatment. We suspect that this should be

doi:10.6342/NTU201903018

the problem of tin-iodide perovskite itself since the most obvious difference between tin perovskite and lead perovskite is stability. The post-treatment is similar to the way of ion exchange method, besides, the ion exchange method involves breaking the bond and then re-bonding. For lead perovskite, it can withstand the breaking bond and re-bonding process, and it will not generate too many surface defects as well as deep defects. On the contrary, once the tin perovskite breaks the bond, the Sn^{2+} undergoes facile oxidation to its tetravalent state, resulting in the lattice collapsed. Although the PLQY of tin-iodide perovskite nanoplates is improved by post-treatment process, the overall enhancement is still compromised by ion exchange resulting in surface defects.

Table 2.2 The PLQY of pre- and post-treatment TEA_2SnI_4.

Name	PLQY(%)
Pre-treatment TEA_2SnI_4[a]	19.5
Post-treatment TEA_2SnI_4[b]	6.5
Post-treatment TEA_2SnI_4[c]	13.7

All values of PLQY are in optimized condition. [a] With 7 % NH_4SCN additive. [b] Dissolve NH_4SCN into non-polar solvent (toluene) to form a saturated solution. After centrifuging the prepared pristine perovskites, the upper solution is removed. The remaining perovskites were suspended in a saturated NH_4SCN solution again and continually stirred for 30 minutes. [c] Adding extra 2 μL 1 M NH_4SCN solution (DMF) in

doi:10.6342/NTU201903018

the prepared pristine perovskites and continually stirring 5 minutes.

The photophysical properties of tin perovskite nanoplates with different proportion NH_4SCN are summarized and showed below (Figure 4.8 and Table 2.3). According to the relationship formula $PLQY = k_r/(k_r + k_{nr}) = k_r \times \tau_{ob}$ where k_r and k_{nr} indicate the radiative rate ($k_r = 1/\tau_r$, τ_r: radiative lifetime) and non-radiative decay rate constants, respectively, and the observed lifetime (τ_{ob}) is the weight average of τ_1, τ_2, and τ_3. Shorter radiative lifetime means that this sample prefers radiative process and has less defects, which indicates that the photophysical properties of tin-iodide perovskite nanoplates are indeed affected by the surface SCN^- ions. The observed lifetime (τ_{ob}) increases as adding the extra NH_4SCN additive. As the proportion of NH_4SCN additive reaches to 7 %, the observed lifetime and PLQY also reaches their maximum. Also, the shortest radiative lifetime and the largest radiative rate are observed. The radiative lifetime of TEA_2SnI_4 and TEA_2SnI_4 with 5 %,7 %, and 9 % NH_4SCN additive are 2.61 ns, 1.34 ns, 1.26 ns, and 1.34 ns respectively, which reveals that as long as the NH_4SCN additive is added to the perovskite precursor, the tin-iodide perovskite nanoplates prefer radiative process. Moreover, accompanied by enhancement in PLQY, we observed that the PL emission of the sample red shifts by 2 nm following the SCN^- treatment (Figure 4.9), a slightly but consistently observed shift in the PL. We considered that the SCN^- ion coordinate on the

doi:10.6342/NTU201903018

surface of tin-iodide perovskite nanoplates resulting in electronic structure slightly changes. Because tin-iodide perovskite nanoplate have a lower dielectric constant in the metal layer than lead analogy, a slight change in electronic properties or polarization ability may result in a light-emitting performance. Hence, we considered this contribution to such significant enhancements may not only reduce defects, but also change electronic structure. Because some studies elucidated that the exciton binding energy and dielectric constants of 2D perovskite nanoplates with SCN^- coordinated are different relative to pristine 2D perovskite nanoplates, we considered that calculating dielectric constants of organic and inorganic layered may have more explanations for this enhanced phenomenon.

doi:10.6342/NTU201903018

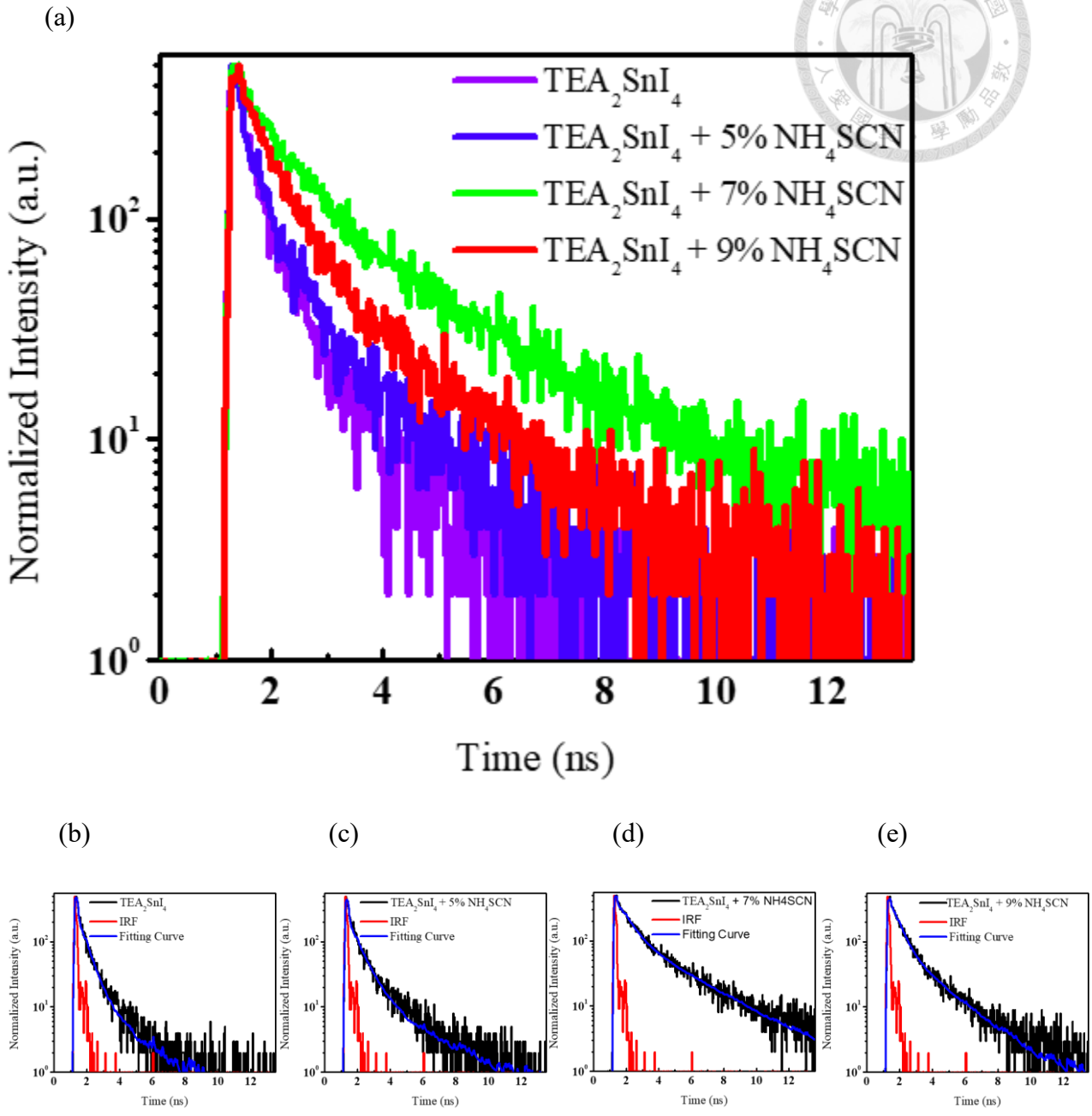

Table 2.3 The photophysical properties of TEA_2SnI_4 with different amount thiocyanate additive.

Name	PLQY (%)	τ1 (ps)		τ2 (ps)		τ3 (ps)		τ_{ob} (ps)	τ_r (ns)	τ_{nr}(ns)	κ_r (ns^{-1})	κ_{nr} (ns^{-1})
TEA_2SnI_4	5.8	63.0	(0.8340)	515.9	(0.1560)	1837	(0.0100)	151.39	2.61	0.160	0.383	6.25
+5%SCN	15.3	76.4	(0.8425)	746.8	(0.1480)	3100	(0.0095)	204.46	1.34	0.241	0.764	4.14
+7%SCN	19.5	22.1	(0.8270)	708.8	(0.1253)	2910	(0.0477)	246.02	1.26	0.305	0.794	3.27
+9%SCN	16.4	23.0	(0.7274)	469.4	(0.2226)	1960	(0.0500)	219.225	1.34	0.262	0.746	3.81

Figure 4.10 Time-resolved photoluminescence measurement of a) merged sample, (b)

doi:10.6342/NTU201903018

TEA_2SnI_4, (c) with 5 %NH_4SCN, (d) with 7 %NH_4SCN, and (e) with 9 %NH_4SCN perovskite nanoplates dispersed in toluene, respectively.

The absorbance at the excitation wavelength (400 nm) was prepared to be ~ 0.1 to avoid reabsorption of the emission.

Table 2.4 Photoluminescence properties of tin perovskite nanodisks in toluene (ex = 400 nm). The values in parentheses indicate the individual contribution percentage of the integral area of fitting curves. The average observed lifetime (τ_{ob}) was defined by weighted average of lifetime according to integral area percentage. The radiative lifetime (τ_r) was equal to τ_{ob}/ PLQY.

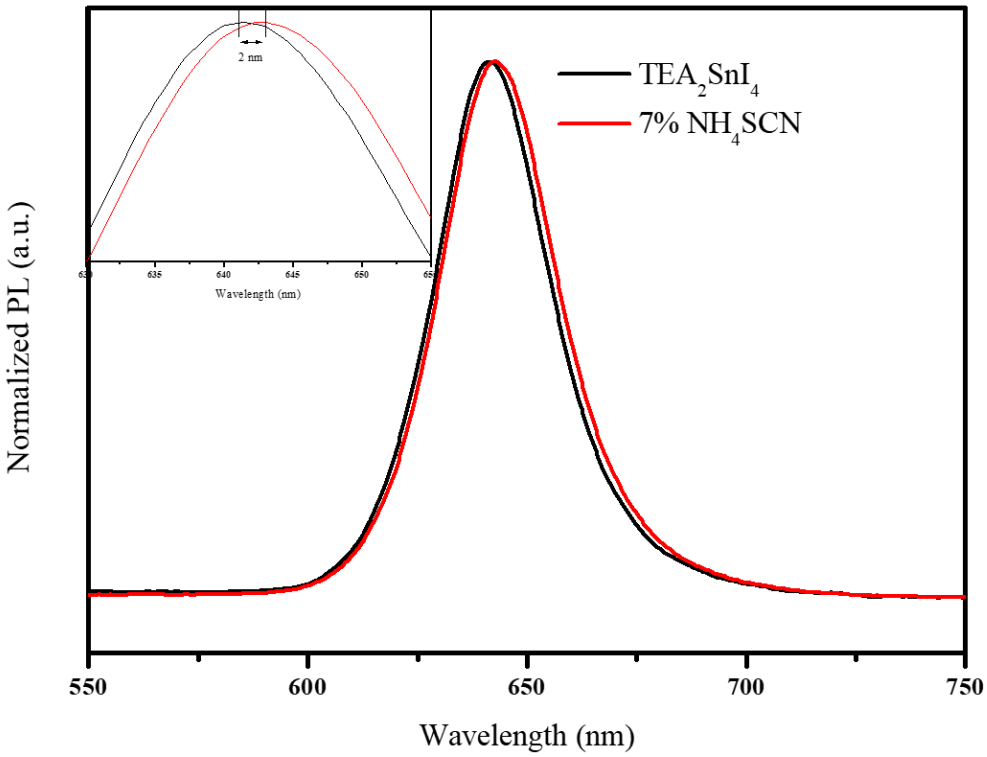

Figure 4.11 The normalized PL spectrum of TEA_2SnI_4 and TEA_2SnI_4 with 7% NH_4SCN.

doi:10.6342/NTU201903018

The dielectric constants of well and barrier layers were estimated using a neutralized ghost-layer model under the independent particle approximation. Details of the computational methodology and simulated structures are explained in SI. To approximate the actual condition of TEA_2SnI_4 / $TEA_2SnI_{4-x}SCN_x$ core-shell, we used TEA_2SnI_4 unit cell and substitute one and two layers +Z direction all iodides to SCN ions (**Figure 4.12**).

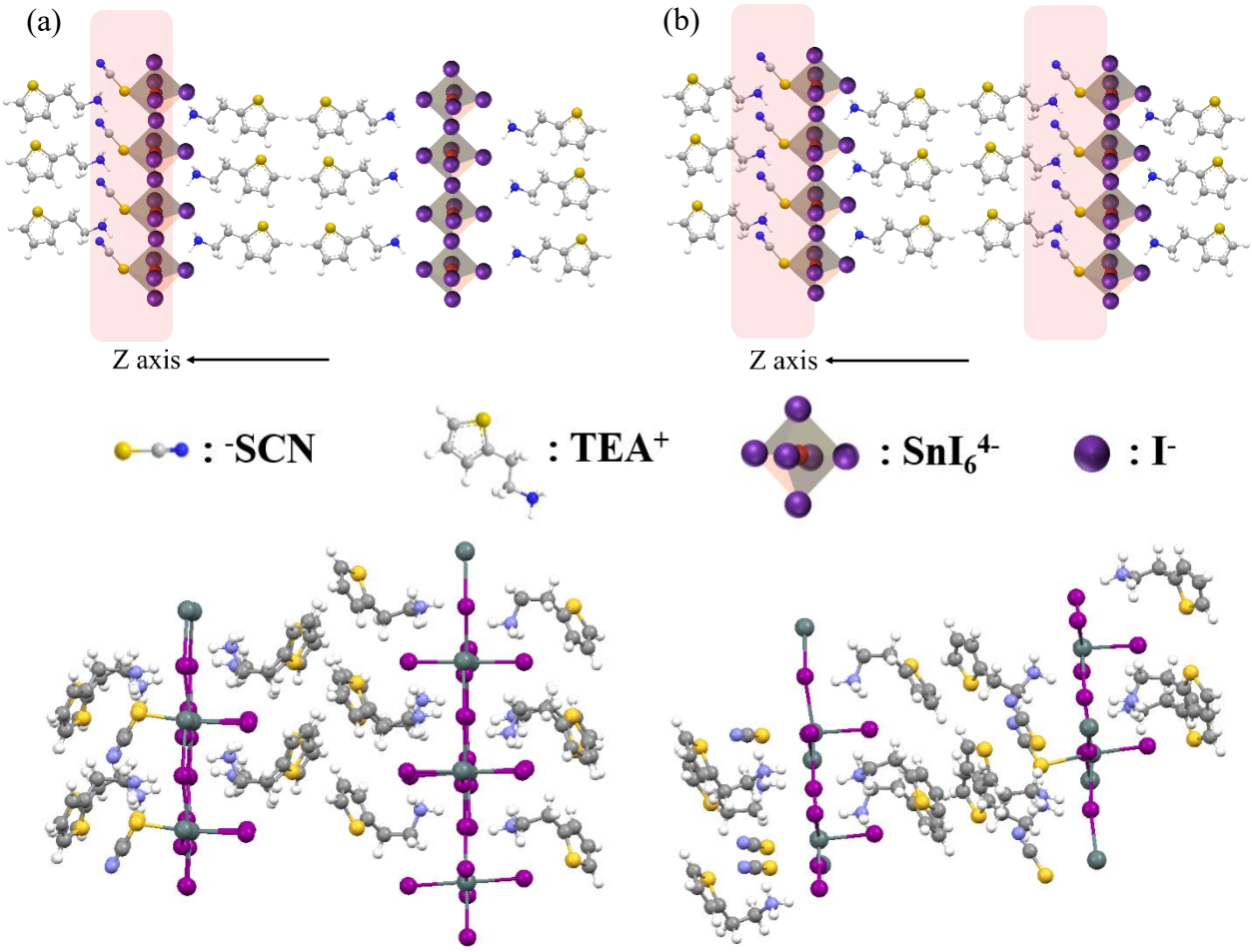

Figure 4.12. Simulated (a) one layer +Z direction substitution and (b) two layers +Z direction substitution.

doi:10.6342/NTU201903018

Because dielectric constant calculated by computer is the result of an average state, using one layer +Z direction SCN ions substituting cannot understand the internal and external layered tin perovskites situation. Hence, two layers of +Z direction SCN ions substitution are necessary, whose dielectric constants represent independent external layered tin perovskites condition. Dielectric constants of one layer +Z direction substitution represent the average of external and internal layered perovskites. Here, we can define dielectric constants of internal layered tin perovskite as A, external layered as B, provided by two layers of +Z direction substitution, and average of external and internal as C, offered by one layer of +Z direction substitution. Those definitions are illustrated at Figure 4.13.

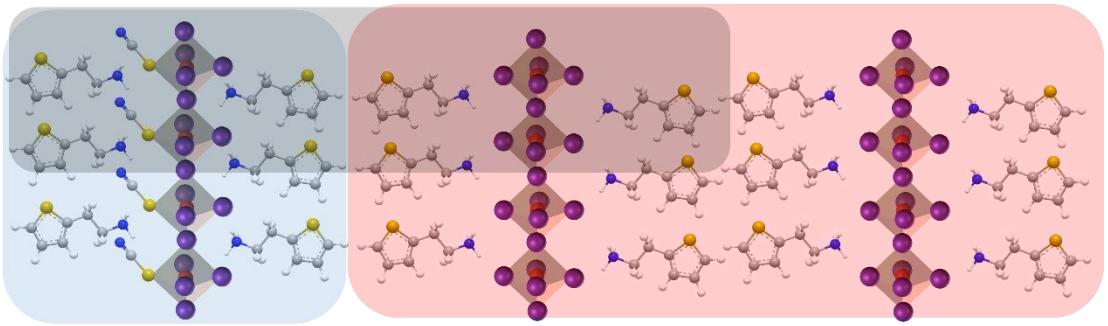

Figure 4.13. Scheme is the illustration of defined A (red region), B (blue region), and C (gray region), respectively.

doi:10.6342/NTU201903018

Following above illustrations, the value C is equal to $\frac{A+B}{2}$, and the unknown value A can be derived by 2×C - B = A. As the result shows, the one layer of +Z direction substitution dielectric constants of the organic layers and inorganic layers are 1.73 and 2.96, respectively, and corresponding values of two layer +Z direction substitution are 1.73 and 2.82, respectively (Table 2.4). Besides, the internal layered tin perovskites corresponding values are 1.73 and 3.10, respectively. Surprisingly, we found that perovskites inorganic layer with bonded SCN ions have lower dielectric constant, but the internal inorganic layer exhibits higher dielectric constant. These results show that though tin layered perovskites bonded with SCN^- have lower polarization, but internal TEA_2SnI_4 has higher polarization. This phenomenon may another result of enhancement of PLQY.

Table 2.4 The dielectric constants of organic and inorganic layer for pristine TEA_2SnI_4, two layer +Z direction substitution TEA_2SnI_4, one layer +Z direction substitution TEA_2SnI_4 and actual condition, respectively.

	ε_b (Org)	ε_w (Inorg)	w/b
TEA	1.64	2.88	1.756
1 layer_+Z	1.73	2.96	1.711
2 layer_+Z	1.73	2.82	1.630
Actual Conditions	1.73	3.10	1.792

doi:10.6342/NTU201903018

According to our computational results, we considered that fewer nanoplates stack should improve photoluminescence because the electric field of excitons can penetrate to outer tin perovskite nanoplates with SCN^- which have lower dielectric constant and be illustrated by Figure 4.13. Hence, the atomic force microscope (AFM) images of tin iodide perovskite nanoplates (see Figure 4.14) illustrate the thickness. The thickness of pristine TEA_2SnI_4 is approximately 17 nm, and with 7 % SCN^- product is about 7 nm.

(a) Thick stacking (b) Thin stacking

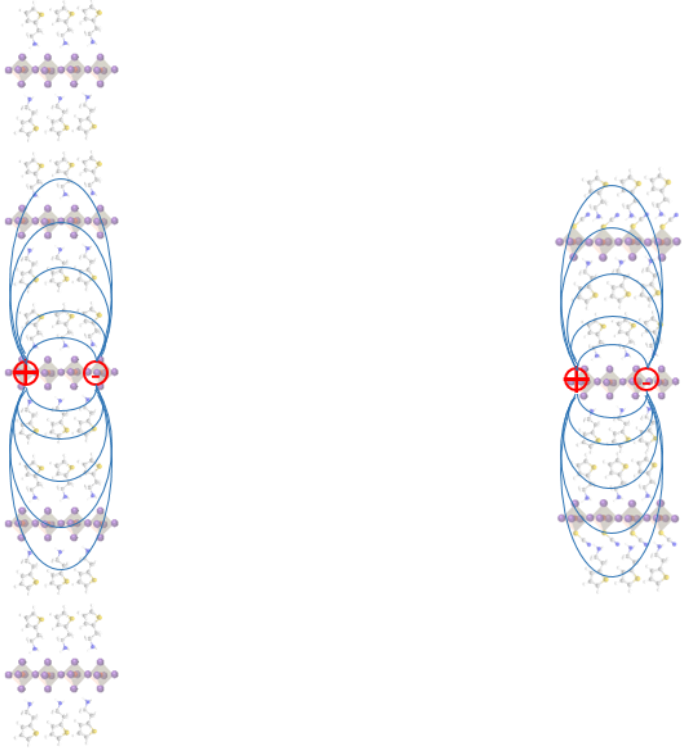

Figure 4.13 Scheme of (a) thick stacking and (b) thin stacking nanoplates.

Red balls mean exciton and blue line means electric field.

doi:10.6342/NTU201903018

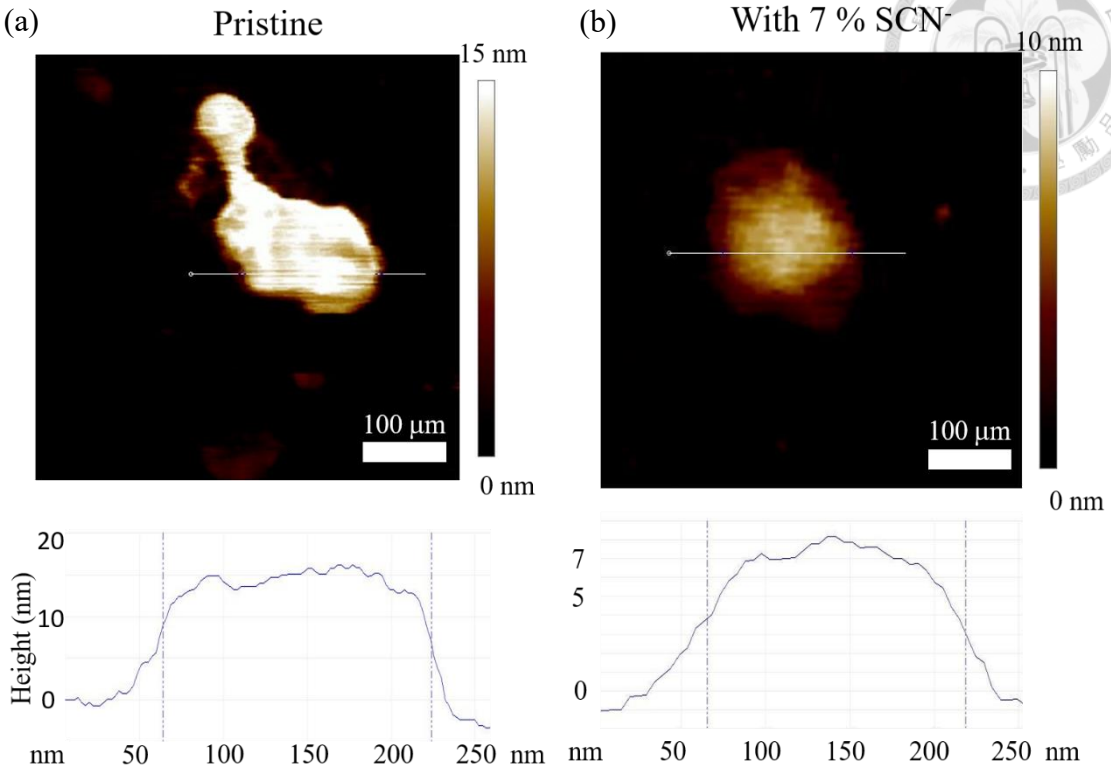

Figure 4.14 AFM images of (a) pristine TEA_2SnI_4 and (b) with 7 SCN^-.

doi:10.6342/NTU201903018

In addition, XPS has also use to test tin-iodide perovskite nanoplates oxidation stability (Figure 4.15). The propensity for the oxidation of Sn^{2+} to Sn^{4+} is notable suppression when TEA_2SnI_4 prepared with NH_4SCN. Upon exposure of TEA_2SnI_4 prepared with 7 % NH_4SCN to air for 30 minutes (Figure 4.15 (e, f) and Table 2.5 (c)), the integral area of Sn^{4+} increase from 4.1 % to 5.54 %. In contrast, under identical conditions, pristine TEA_2SnI_4 that synthesized without NH_4SCN (Figure 4.15 (a, b) and Table 2.5 (a)) showed the integral area of Sn^{4+} increase from 8.06 % to 23.66 %. By using our last report's strategy, TEA_2SnI_4 nanoplate was synthesized with 0.1 vol % pentanoic acid additive (Figure 4.15 (c, d) and Table 2.5 (b)) showed the integral area of Sn^{4+} increase from 7.15 % to 15.90 %. This significant improvement of air stability is incredible. We suspected that the surface of tin-iodide perovskite nanoplates, where the trace amount of SCN^- ion exists, can effectively prevent Sn^{2+} from oxidizing due to strong chemical interaction between SCN^- and Sn^{2+}.

doi:10.6342/NTU201903018

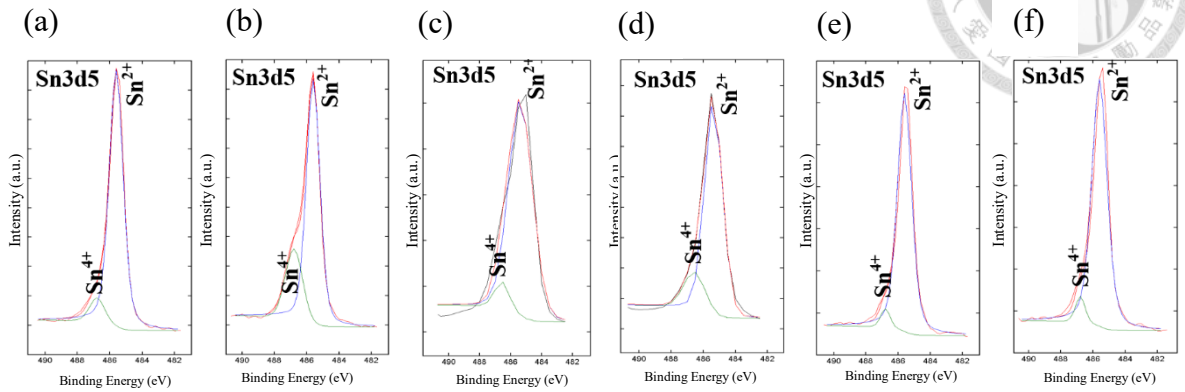

Figure 4.15 X-ray photoelectron spectroscopy for TEA_2SnI_4 before (a, c, e) and after (b, d, f) exposure to air for 30 minutes. The Sn^{4+} signal observed in the sample without 30 minutes of air exposure could arise during loading process. (a, b) Pristine TEA_2SnI_4 nanoplates (c, d) TEA_2SnI_4 nanoplate with 0.1 vol % pentanoic acid additive (e, f) TEA_2SnI_4 nanoplate with 7% NH_4SCN additive.

Table 2.5 Content analysis of Sn^{2+} and Sn^{4+} from Sn 3d5/2 spectra for (a) pristine TEA_2SnI_4, (b) TEA_2SnI_4 nanoplate with 0.1 vol % pentanoic acid additive, (c) TEA_2SnI_4 nanoplate with 7% NH_4SCN additive.

(a)

Exposure to air for 30 min	Element value number	Binding energy (eV)	Area (%)
Before	Sn^{2+}	485.5	91.94
	Sn^{4+}	486.7	8.06
After	Sn^{2+}	485.5	76.34
	Sn^{4+}	486.7	23.66

(b)

Exposure to air for 30 min	Element value number	Binding energy (eV)	Area (%)
Before	Sn^{2+}	485.5	92.85
	Sn^{4+}	486.7	7.15
After	Sn^{2+}	485.5	84.10
	Sn^{4+}	486.7	15.90

(c)

Exposure to air for 30 min	Element value number	Binding energy (eV)	Area (%)
Before	Sn^{2+}	485.5	95.9
	Sn^{4+}	486.7	4.1
After	Sn^{2+}	485.5	94.55
	Sn^{4+}	486.7	5.45

doi:10.6342/NTU201903018

Furthermore, the photostability for TEA_2SnI_4 under ambient condition with continuous 375 nm (10 mW cm^{-2}) illumination exhibited the similar trend (Figure 4.16). This significant improvement of air stability is incredible. We considered that the surface of tin-iodide perovskite nanoplates, where the trace amount of SCN ion exists, can effectively prevent Sn^{2+} from oxidizing due to strong chemical interaction between SCN^- and Sn^{2+}.

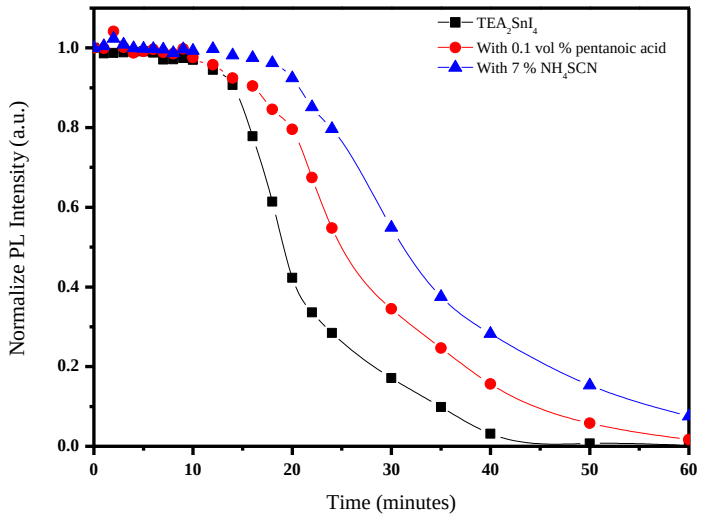

Figure 4.16. Photostability test for pristine TEA_2SnI_4 (black line), with 0.1 vol% pentanoic acid (red line), and with 7 % NH_4SCN (blue line) in air under continuous 375 nm (10 mW/cm_2) illumination.

doi:10.6342/NTU201903018

Chapter 7 Conclusion

According to our research, we found that SCN^- additives can effectively prevent the surface of tin-iodide perovskite nanoplates from oxidizing. We have inferred the core-shell like tin-iodide perovskite nanoplates by XRD, XPS and ToF-SIMS results. In addition, the results of XPS illustrated that this structure has excellent air stability. Besides, we discussed the dielectric constant of this core-shell like tin-iodide perovskite nanoplates. From the results of computational methodology, we can understand that on the tin-iodide perovskite nanoplates where SCN^- coordinating on the surface has weaker dielectric confinement effect, but the internal tin-iodide perovskite nanoplates has higher dielectric confinement effect than pristine TEA_2SnI_4. Based on the above results, we can infer that the functions of the additive not only fill in the surface defects (or passivate surface of tin-iodide perovskite nanoplates), but also change the electronic structure of the tin-iodide perovskite nanoplates. Hence, we can obtain the such high PLQY and excellent air stability.

doi:10.6342/NTU201903018

Reference

1. Kojima, A.; Teshima, K.; Shirai, Y.; Miyasaka, T., Organometal Halide Perovskites as Visible-Light Sensitizers for Photovoltaic Cells. *Journal of the American Chemical Society* **2009**, 6050-6051.

2. Bi, D.; Yi, C.; Luo, J.; Décoppet, J.-D.; Zhang, F.; Zakeeruddin, Shaik M.; Li, X.; Hagfeldt, A.; Grätzel, M., Polymer-templated nucleation and crystal growth of perovskite films for solar cells with efficiency greater than 21%. *Nature Energy* **2016**, 16142.

3. Zhao, D.; Wang, C.; Song, Z.; Yu, Y.; Chen, C.; Zhao, X.; Zhu, K.; Yan, Y., Four-Terminal All-Perovskite Tandem Solar Cells Achieving Power Conversion Efficiencies Exceeding 23%. *ACS Energy Letters* **2018**, 305-306.

4. Era, M.; Morimoto, S.; Tsutsui, T.; Saito, S., Organic-inorganic heterostructure electroluminescent device using a layered perovskite semiconductor $(C_6H_5C_2H_4NH_3)_2PbI_4$. *Applied Physics Letters* **1994**, 676-678.

5. Tan, Z.-K.; Moghaddam, R. S.; Lai, M. L.; Docampo, P.; Higler, R.; Deschler, F.; Price, M.; Sadhanala, A.; Pazos, L. M.; Credgington, D.; Hanusch, F.; Bein, T.; Snaith, H. J.; Friend, R. H., Bright light-emitting diodes based on organometal halide perovskite. *Nature Nanotechnology* **2014**, 687.

doi:10.6342/NTU201903018

6. Cho, H.; Jeong, S.-H.; Park, M.-H.; Kim, Y.-H.; Wolf, C.; Lee, C.-L.; Heo, J. H.; Sadhanala, A.; Myoung, N.; Yoo, S.; Im, S. H.; Friend, R. H.; Lee, T.-W., Overcoming the electroluminescence efficiency limitations of perovskite light-emitting diodes. *Science* **2015**, 1222.

7. Wang, N.; Cheng, L.; Ge, R.; Zhang, S.; Miao, Y.; Zou, W.; Yi, C.; Sun, Y.; Cao, Y.; Yang, R.; Wei, Y.; Guo, Q.; Ke, Y.; Yu, M.; Jin, Y.; Liu, Y.; Ding, Q.; Di, D.; Yang, L.; Xing, G.; Tian, H.; Jin, C.; Gao, F.; Friend, R. H.; Wang, J.; Huang, W., Perovskite light-emitting diodes based on solution-processed self-organized multiple quantum wells. *Nature Photonics* **2016**, 699.

8. Dou, L.; Yang, Y.; You, J.; Hong, Z.; Chang, W.-H.; Li, G.; Yang, Y., Solution-processed hybrid perovskite photodetectors with high detectivity. *Nature Communications* **2014**, 5404.

9. Wei, H.; Fang, Y.; Mulligan, P.; Chuirazzi, W.; Fang, H.-H.; Wang, C.; Ecker, B. R.; Gao, Y.; Loi, M. A.; Cao, L.; Huang, J., Sensitive X-ray detectors made of methylammonium lead tribromide perovskite single crystals. *Nature Photonics* **2016**, 333.

10. Yakunin, S.; Sytnyk, M.; Kriegner, D.; Shrestha, S.; Richter, M.; Matt, G. J.; Azimi, H.; Brabec, C. J.; Stangl, J.; Kovalenko, M. V.; Heiss, W., Detection of X-ray

doi:10.6342/NTU201903018

photons by solution-processed lead halide perovskites. *Nature Photonics* **2015**, 444.

11. Zhu, H.; Fu, Y.; Meng, F.; Wu, X.; Gong, Z.; Ding, Q.; Gustafsson, M. V.; Trinh, M. T.; Jin, S.; Zhu, X. Y., Lead halide perovskite nanowire lasers with low lasing thresholds and high quality factors. *Nature Materials* **2015**, 636.

12. Lufaso, M. W.; Woodward, P. M., Jahn-Teller distortions, cation ordering and octahedral tilting in perovskites. *Acta Crystallographica Section B* **2004**, 10-20.

13. Glazer, A., The classification of tilted octahedra in perovskites. *Acta Crystallographica Section B* **1972**, 3384-3392.

14. Stoumpos, C. C.; Malliakas, C. D.; Kanatzidis, M. G., Semiconducting Tin and Lead Iodide Perovskites with Organic Cations: Phase Transitions, High Mobilities, and Near-Infrared Photoluminescent Properties. *Inorganic Chemistry* **2013**, 9019-9038.

15. Krishnamoorthy, T.; Ding, H.; Yan, C.; Leong, W. L.; Baikie, T.; Zhang, Z.; Sherburne, M.; Li, S.; Asta, M.; Mathews, N.; Mhaisalkar, S. G., Lead-free germanium iodide perovskite materials for photovoltaic applications. *Journal of Materials Chemistry A* **2015**, 23829-23832.

16. Yangui, A.; Pillet, S.; Bendeif, E.-E.; Lusson, A.; Triki, S.; Abid, Y.; Boukheddaden, K., Broadband Emission in a New Two-Dimensional Cd-Based Hybrid Perovskite. *ACS Photonics* **2018**, 1599-1611.

doi:10.6342/NTU201903018

17. Needham, G.; Willett, R.; Franzen, H. J. T. J. o. P. C., Phase transitions in crystalline models of bilayers. 1. Differential scanning calorimetric and x-ray studies of $(C_{12}H_{25}NH_3)_2MCl_4$ and $(NH_3C1_4H_{29}NH_3)_2MCl_4$ salts (M= Mn^{2+}, Cd^{2+}, Cu^{2+}). *The Jornal of Physical* **1984**, 674-680.

18. Shi, D.; Adinolfi, V.; Comin, R.; Yuan, M.; Alarousu, E.; Buin, A.; Chen, Y.; Hoogland, S.; Rothenberger, A.; Katsiev, K.; Losovyj, Y.; Zhang, X.; Dowben, P. A.; Mohammed, O. F.; Sargent, E. H.; Bakr, O. M., Low trap-state density and long carrier diffusion in organolead trihalide perovskite single crystals. *Science* **2015**, 519.

19. Saidaminov, M. I.; Abdelhady, A. L.; Murali, B.; Alarousu, E.; Burlakov, V. M.; Peng, W.; Dursun, I.; Wang, L.; He, Y.; Maculan, G.; Goriely, A.; Wu, T.; Mohammed, O. F.; Bakr, O. M., High-quality bulk hybrid perovskite single crystals within minutes by inverse temperature crystallization. *Nature Communications* **2015**, 7586.

20. Han, Q.; Bae, S.-H.; Sun, P.; Hsieh, Y.-T.; Yang, Y.; Rim, Y. S.; Zhao, H.; Chen, Q.; Shi, W.; Li, G.; Yang, Y., Single Crystal Formamidinium Lead Iodide ($FAPbI_3$): Insight into the Structural, Optical, and Electrical Properties. *Advanced Materials* **2016**, 2253-2258.

21. Kieslich, G.; Sun, S.; Cheetham, A. K., Solid-state principles applied to organic–inorganic perovskites: new tricks for an old dog. *Chemical Science* **2014**, 4712-4715.

doi:10.6342/NTU201903018

22. Mitzi, D. B., Templating and structural engineering in organic–inorganic perovskites. *Journal of the Chemical Society, Dalton Transactions* **2001**, 1-12.

23. Saparov, B.; Mitzi, D. B., Organic–Inorganic Perovskites: Structural Versatility for Functional Materials Design. *Chemical Reviews* **2016**, 4558-4596.

24. Dohner, E. R.; Hoke, E. T.; Karunadasa, H. I., Self-Assembly of Broadband White-Light Emitters. *Journal of the American Chemical Society* **2014**, 1718-1721.

25. Vargas, B.; Ramos, E.; Pérez-Gutiérrez, E.; Alonso, J. C.; Solis-Ibarra, D., A Direct Bandgap Copper–Antimony Halide Perovskite. *Journal of the American Chemical Society* **2017**, 9116-9119.

26. Nazarenko, O.; Kotyrba, M. R.; Yakunin, S.; Aebli, M.; Rainò, G.; Benin, B. M.; Wörle, M.; Kovalenko, M. V., Guanidinium-Formamidinium Lead Iodide: A Layered Perovskite-Related Compound with Red Luminescence at Room Temperature. *Journal of the American Chemical Society* **2018**, 3850-3853.

27. Mao, L.; Wu, Y.; Stoumpos, C. C.; Wasielewski, M. R.; Kanatzidis, M. G., White-Light Emission and Structural Distortion in New Corrugated Two-Dimensional Lead Bromide Perovskites. *Journal of the American Chemical Society* **2017**, 5210-5215.

28. Guan, J.; Tang, Z.; M. Guloy, A., α-$[NH_3(CH_2)_5NH_3]SnI_4$: a new layered perovskite structure. *Chemical Communications* **1999**, 1833-1834.

doi:10.6342/NTU201903018

29. Dou, L.; Wong, A. B.; Yu, Y.; Lai, M.; Kornienko, N.; Eaton, S. W.; Fu, A.; Bischak, C. G.; Ma, J.; Ding, T.; Ginsberg, N. S.; Wang, L.-W.; Alivisatos, A. P.; Yang, P., Atomically thin two-dimensional organic-inorganic hybrid perovskites. *Science* **2015**, 1518.

30. Mitzi, D. B.; Dimitrakopoulos, C. D.; Kosbar, L. L., Structurally Tailored Organic−Inorganic Perovskites: Optical Properties and Solution-Processed Channel Materials for Thin-Film Transistors. *Chemistry of Materials* **2001**, 3728-3740.

31. Knutson, J. L.; Martin, J. D.; Mitzi, D. B., Tuning the Band Gap in Hybrid Tin Iodide Perovskite Semiconductors Using Structural Templating. *Inorganic Chemistry* **2005**, 4699-4705.

32. Lermer, C.; Birkhold, S. T.; Moudrakovski, I. L.; Mayer, P.; Schoop, L. M.; Schmidt-Mende, L.; Lotsch, B. V., Toward Fluorinated Spacers for MAPI-Derived Hybrid Perovskites: Synthesis, Characterization, and Phase Transitions of $(FC_2H_4NH_3)_2PbCl_4$. *Chemistry of Materials* **2016**, 6560-6566.

33. Thomson, R. I.; Rawson, J. M.; Goeta, A.; Probert, M. R.; Coome, J. A.; Hoang, T. K. A.; Carpenter, M. A., Elastic coupling and anelastic relaxation associated with multiple phase transitions in para-chloroanilinium tetrachlorocuprate, $[p\text{-}ClC_6H_4NH_3]_2CuCl_4$. *Materials Chemistry and Physics* **2013**, 34-46.

doi:10.6342/NTU201903018

34. Pan, X.-w.; Wu, G.; Wang, M.; Chen, H.-z., Partially reversible photochromic behavior of organic-inorganic perovskites with copper(II) chloride. *Journal of Zhejiang University-SCIENCE A* **2009**, 710-715.

35. Mostafa, M. F.; Abdel-Kader, M. M.; Arafat, S. S.; Kandeel, E. M., Thermochromic phase transitions in two aromatic tetrachlorocuprates. *Physica Scripta* **1991**, 627-629.

36. Xu, Z.; Mitzi, D. B.; Dimitrakopoulos, C. D.; Maxcy, K. R., Semiconducting Perovskites $(2\text{-}XC_6H_4C_2H_4NH_3)_2SnI_4$ (X = F, Cl, Br): Steric Interaction between the Organic and Inorganic Layers. *Inorganic Chemistry* **2003**, 2031-2039.

37. Xu, Z.; Mitzi, D. B.; Medeiros, D. R., $[(CH_3)_3NCH_2CH_2NH_3]SnI_4$: A Layered Perovskite with Quaternary/Primary Ammonium Dications and Short Interlayer Iodine−Iodine Contacts. *Inorganic Chemistry* **2003**, 1400-1402.

38. Du, K.-z.; Tu, Q.; Zhang, X.; Han, Q.; Liu, J.; Zauscher, S.; Mitzi, D. B., Two-Dimensional Lead(II) Halide-Based Hybrid Perovskites Templated by Acene Alkylamines: Crystal Structures, Optical Properties, and Piezoelectricity. *Inorganic Chemistry* **2017**, 9291-9302.

39. Calabrese, J.; Jones, N. L.; Harlow, R. L.; Herron, N.; Thorn, D. L.; Wang, Y., Preparation and characterization of layered lead halide compounds. *Journal of the*

doi:10.6342/NTU201903018

American Chemical Society **1991**, 2328-2330.

40. Mitzi, D. B.; Wang, S.; Feild, C. A.; Chess, C. A.; Guloy, A. M., Conducting Layered Organic-inorganic Halides Containing <110>-Oriented Perovskite Sheets. *Science* **1995**, 1473.

41. Stoumpos, C. C.; Soe, C. M. M.; Tsai, H.; Nie, W.; Blancon, J.-C.; Cao, D. H.; Liu, F.; Traoré, B.; Katan, C.; Even, J.; Mohite, A. D.; Kanatzidis, M. G., High Members of the 2D Ruddlesden-Popper Halide Perovskites: Synthesis, Optical Properties, and Solar Cells of $(CH_3(CH_2)_3NH_3)_2(CH_3NH_3)_4Pb_5I_{16}$. *Chem* **2017**, 427-440.

42. Stoumpos, C. C.; Cao, D. H.; Clark, D. J.; Young, J.; Rondinelli, J. M.; Jang, J. I.; Hupp, J. T.; Kanatzidis, M. G., Ruddlesden–Popper Hybrid Lead Iodide Perovskite 2D Homologous Semiconductors. *Chemistry of Materials* **2016**, 2852-2867.

43. Dolzhenko, Y. I.; Inabe, T.; Maruyama, Y., In Situ X-Ray Observation on the Intercalation of Weak Interaction Molecules into Perovskite-Type Layered Crystals $(C_9H_{19}NH_3)_2PbI_4$ and $(C_{10}H_{21}NH_3)_2CdCl_4$. *Bulletin of the Chemical Society of Japan* **1986**, 563-567.

44. Papavassiliou, G. C.; Koutselas, J. B.; Lagouvardos, D. J., Notizen: Preparation and Characterization of $(C_6H_5CH_2CH_2NH_3)_2SnI_4$ and $(C_6H_5CH_2CH_2NH_3)_2SnBr_4$. In *Zeitschrift für Naturforschung B*, 1993; 1013.

doi:10.6342/NTU201903018

45. Mitzi, D. B., Synthesis, Crystal Structure, and Optical and Thermal Properties of $(C_4H_9NH_3)_2MI_4$ (M = Ge, Sn, Pb). *Chemistry of Materials* **1996,** 791-800.

46. Cortecchia, D.; Dewi, H. A.; Yin, J.; Bruno, A.; Chen, S.; Baikie, T.; Boix, P. P.; Grätzel, M.; Mhaisalkar, S.; Soci, C.; Mathews, N., Lead-Free $MA_2CuCl_xBr_{4-x}$ Hybrid Perovskites. *Inorganic Chemistry* **2016,** 1044-1052.

47. Arend, H.; Tichy, K.; Baberschke, K.; Rys, F., Chloride perovskite layer compounds of $[NH_3\text{-}(CH_2)_n\text{-}NH_3]MnCl_4$ formula. *Solid State Communications* **1976,** 999-1003.

48. Han, J.; Nishihara, S.; Inoue, K.; Kurmoo, M., On the Nature of the Structural and Magnetic Phase Transitions in the Layered Perovskite-Like $(CH_3NH_3)_2[Fe^{II}Cl_4]$. *Inorganic Chemistry* **2014**, 2068-2075.

49. Mitzi, D. B.; Liang, K., Preparation and Properties of $(C_4H_9NH_3)_2EuI_4$: A Luminescent Organic−Inorganic Perovskite with a Divalent Rare-Earth Metal Halide Framework. *Chemistry of Materials* **1997,** 2990-2995.

50. Mitzi, D. B., Organic−Inorganic Perovskites Containing Trivalent Metal Halide Layers: The Templating Influence of the Organic Cation Layer. *Inorganic Chemistry* **2000,** 6107-6113.

51. Castro-Castro, L. M.; Guloy, A. M., Organic-Based Layered Perovskites of Mixed-

doi:10.6342/NTU201903018

Valent Gold(I)/Gold(III) Iodides. *Angewandte Chemie International Edition* **2003**, 2771-2774.

52. Connor, B. A.; Leppert, L.; Smith, M. D.; Neaton, J. B.; Karunadasa, H. I., Layered Halide Double Perovskites: Dimensional Reduction of $Cs_2AgBiBr_6$. *Journal of the American Chemical Society* **2018,** 5235-5240.

53. Kitazawa, N., Excitons in two-dimensional layered perovskite compounds: $(C_6H_5C_2H_4NH_3)_2Pb(Br,I)_4$ and $(C_6H_5C_2H_4NH_3)_2Pb(Cl,Br)_4$. *Materials Science and Engineering: B* **1997,** 233-238.

54. Kitazawa, N., Optical Absorption and Photoluminescence Properties of Pb(I, Br)-Based Two-Dimensional Layered Perovskite. *Japanese Journal of Applied Physics* **1997**, 2272-2276.

55. Kitazawa, N., Compositional Modulation of Two-Dimensional Layered Perovskite$(RNH_3)_2Pb(Cl,Br,I)_4$and Its Optical Properties. *Japanese Journal of Applied Physics* **1996**, 6202-6207.

56. Daub, M.; Hillebrecht, H., Synthesis, Single-Crystal Structure and Characterization of $(CH_3NH_3)_2Pb(SCN)_2I_2$. *Angewandte Chemie International Edition* **2015**, 11016-11017.

57. Muljarov, E. A.; Tikhodeev, S. G.; Gippius, N. A.; Ishihara, T., Excitons in self-

doi:10.6342/NTU201903018

organized semiconductor/insulator superlattices: PbI-based perovskite compounds. *Physical Review B* **1995**, 14370-14378.

58. Green, M. A.; Jiang, Y.; Soufiani, A. M.; Ho-Baillie, A., Optical Properties of Photovoltaic Organic–Inorganic Lead Halide Perovskites. *The Journal of Physical Chemistry Letters* **2015**, 4774-4785.

59. Hong, X.; Ishihara, T.; Nurmikko, A. V., Dielectric confinement effect on excitons in lead-based layered semiconductors. *Physical Review B* **1992**, 6961-6964.

60. Ishihara, T., Optical properties of PbI-based perovskite structures. *Journal of Luminescence* **1994**, 269-274.

61. Lin, Q.; Armin, A.; Nagiri, R. C. R.; Burn, P. L.; Meredith, P., Electro-optics of perovskite solar cells. *Nature Photonics* **2014,** 106.

62. Smith, M. D.; Karunadasa, H. I., White-Light Emission from Layered Halide Perovskites. *Accounts of Chemical Research* **2018**, 619-627.

63. Smith, M. D.; Pedesseau, L.; Kepenekian, M.; Smith, I. C.; Katan, C.; Even, J.; Karunadasa, H. I., Decreasing the electronic confinement in layered perovskites through intercalation. *Chemical Science* **2017**, 1960-1968.

64. Wood, D. L.; Tauc, J., Weak Absorption Tails in Amorphous Semiconductors. *Physical Review B* **1972**, 3144-3151.

doi:10.6342/NTU201903018

65. Dolgonos, A.; Mason, T. O.; Poeppelmeier, K. R., Direct optical band gap measurement in polycrystalline semiconductors: A critical look at the Tauc method. *Journal of Solid State Chemistry* **2016**, 43-48.

66. Straus, D. B.; Kagan, C. R., Electrons, Excitons, and Phonons in Two-Dimensional Hybrid Perovskites: Connecting Structural, Optical, and Electronic Properties. *The Journal of Physical Chemistry Letters* **2018**, 1434-1447.

67. Takagi, H.; Kunugita, H.; Ema, K., Influence of the image charge effect on excitonic energy structure in organic-inorganic multiple quantum well crystals. *Physical Review B* **2013**, 125421.

68. Umeyama, D.; Lin, Y.; Karunadasa, H. I., Red-to-Black Piezochromism in a Compressible Pb–I–SCN Layered Perovskite. *Chemistry of Materials* **2016**, 3241-3244.

69. Smith, I. C.; Hoke, E. T.; Solis-Ibarra, D.; McGehee, M. D.; Karunadasa, H. I., A Layered Hybrid Perovskite Solar-Cell Absorber with Enhanced Moisture Stability. *Angewandte Chemie International Edition* **2014**, 11232-11235.

70. Hoefler, S. F.; Trimmel, G.; Rath, T., Progress on lead-free metal halide perovskites for photovoltaic applications: a review. *Monatshefte für Chemie - Chemical Monthly* **2017**, 795-826.

71. Shannon, R., Revised effective ionic radii and systematic studies of interatomic

doi:10.6342/NTU201903018

distances in halides and chalcogenides. *Acta Crystallographica Section A* **1976**, 751-767.

72. Manser, J. S.; Christians, J. A.; Kamat, P. V., Intriguing Optoelectronic Properties of Metal Halide Perovskites. *Chemical Reviews* **2016**, 12956-13008.

73. Song, T.-B.; Yokoyama, T.; Aramaki, S.; Kanatzidis, M. G., Performance Enhancement of Lead-Free Tin-Based Perovskite Solar Cells with Reducing Atmosphere-Assisted Dispersible Additive. *ACS Energy Letters* **2017**, 897-903.

74. Marshall, K. P.; Walker, M.; Walton, R. I.; Hatton, R. A., Enhanced stability and efficiency in hole-transport-layer-free CsSnI3 perovskite photovoltaics. *Nature Energy* **2016**, 16178.

75. Song, T.-B.; Yokoyama, T.; Stoumpos, C. C.; Logsdon, J.; Cao, D. H.; Wasielewski, M. R.; Aramaki, S.; Kanatzidis, M. G., Importance of Reducing Vapor Atmosphere in the Fabrication of Tin-Based Perovskite Solar Cells. *Journal of the American Chemical Society* **2017**, 836-842.

76. Gupta, S.; Cahen, D.; Hodes, G., How SnF_2 Impacts the Material Properties of Lead-Free Tin Perovskites. *The Journal of Physical Chemistry C* **2018**, 13926-13936.

77. Qin, C.; Matsushima, T.; Fujihara, T.; Adachi, C., Multifunctional Benzoquinone Additive for Efficient and Stable Planar Perovskite Solar Cells. *Advanced Materials*

doi:10.6342/NTU201903018

2017 , 1603808.

78. Li, W.; Li, J.; Li, J.; Fan, J.; Mai, Y.; Wang, L., Addictive-assisted construction of all-inorganic $CsSnIBr_2$ mesoscopic perovskite solar cells with superior thermal stability up to 473 K. *Journal of Materials Chemistry A* **2016** , 17104-17110.

79. Quan, L. N.; Yuan, M.; Comin, R.; Voznyy, O.; Beauregard, E. M.; Hoogland, S.; Buin, A.; Kirmani, A. R.; Zhao, K.; Amassian, A.; Kim, D. H.; Sargent, E. H., Ligand-Stabilized Reduced-Dimensionality Perovskites. *Journal of the American Chemical Society* **2016**, 2649-2655.

80. Sun, P.-P.; Li, Q.-S.; Yang, L.-N.; Li, Z.-S., Theoretical insights into a potential lead-free hybrid perovskite: substituting Pb2+ with Ge2+. *Nanoscale* **2016**, 1503-1512.

81. Tang, L.-C.; Chang, Y.-C.; Huang, J.-Y.; Lee, M.-H.; Chang, C.-S., First Principles Calculations of Linear and Second-Order Optical Responses in Rhombohedrally Distorted Perovskite Ternary Halides, $CsGeX_3$(X = Cl, Br, and I). *Japanese Journal of Applied Physics* **2009**, 112402.

82. Chen, M.; Ju, M.-G.; Garces, H. F.; Carl, A. D.; Ono, L. K.; Hawash, Z.; Zhang, Y.; Shen, T.; Qi, Y.; Grimm, R. L.; Pacifici, D.; Zeng, X. C.; Zhou, Y.; Padture, N. P., Highly stable and efficient all-inorganic lead-free perovskite solar cells with native-oxide passivation. *Nature Communications* **2019** , 16.

doi:10.6342/NTU201903018

83. Jellicoe, T. C.; Richter, J. M.; Glass, H. F. J.; Tabachnyk, M.; Brady, R.; Dutton, S. E.; Rao, A.; Friend, R. H.; Credgington, D.; Greenham, N. C.; Böhm, M. L., Synthesis and Optical Properties of Lead-Free Cesium Tin Halide Perovskite Nanocrystals. *Journal of the American Chemical Society* **2016**, 2941-2944.

84. Weidman, M. C.; Seitz, M.; Stranks, S. D.; Tisdale, W. A., Highly Tunable Colloidal Perovskite Nanoplatelets through Variable Cation, Metal, and Halide Composition. *ACS Nano* **2016**, 7830-7839.

85. Chen, M.-Y.; Lin, J.-T.; Hsu, C.-S.; Chang, C.-K.; Chiu, C.-W.; Chen, H. M.; Chou, P.-T., Strongly Coupled Tin-Halide Perovskites to Modulate Light Emission: Tunable 550–640 nm Light Emission (FWHM 36–80 nm) with a Quantum Yield of up to 6.4%. *Advanced Materials* **2018**, 1706592.

86. Lin, J.-T.; Liao, C.-C.; Hsu, C.-S.; Chen, D.-G.; Chen, H.-M.; Tsai, M.-K.; Chou, P.-T.; Chiu, C.-W., Harnessing Dielectric Confinement on Tin Perovskites to Achieve Emission Quantum Yield up to 21%. *Journal of the American Chemical Society* **2019**, 10324-10330.

87. Koscher, B. A.; Swabeck, J. K.; Bronstein, N. D.; Alivisatos, A. P., Essentially Trap-Free CsPbBr3 Colloidal Nanocrystals by Postsynthetic Thiocyanate Surface Treatment. *Journal of the American Chemical Society* **2017**, 6566-6569.

doi:10.6342/NTU201903018

88. Zhang, J.; Wu, S.; Liu, T.; Zhu, Z.; Jen, A. K. Y., Boosting Photovoltaic Performance for Lead Halide Perovskites Solar Cells with BF_4^- Anion Substitutions. *Advanced Functional Materials* **2019**, 1808833.

89. Ahmed, T.; Seth, S.; Samanta, A., Boosting the Photoluminescence of $CsPbX_3$ (X = Cl, Br, I) Perovskite Nanocrystals Covering a Wide Wavelength Range by Postsynthetic Treatment with Tetrafluoroborate Salts. *Chemistry of Materials* **2018**, 3633-3637.

90. Chen, J.; Kim, S.-G.; Park, N.-G., $FA_{0.88}Cs_{0.12}PbI_{3-x}(PF_6)_x$ Interlayer Formed by Ion Exchange Reaction between Perovskite and Hole Transporting Layer for Improving Photovoltaic Performance and Stability. *Advanced Materials* **2018**, 1801948.

91. Kim, H.; Lee, Y. H.; Lyu, T.; Yoo, J. H.; Park, T.; Oh, J. H., Boosting the performance and stability of quasi-two-dimensional tin-based perovskite solar cells using the formamidinium thiocyanate additive. *Journal of Materials Chemistry A* **2018**, 18173-18182.

92. Jeon, N. J.; Noh, J. H.; Kim, Y. C.; Yang, W. S.; Ryu, S.; Seok, S. I., Solvent engineering for high-performance inorganic–organic hybrid perovskite solar cells. *Nature Materials* **2014**, 897.

93. Fang, H.; Jena, P., Atomic-Level Design of Water-Resistant Hybrid Perovskites for

doi:10.6342/NTU201903018

Solar Cells by Using Cluster Ions. *The Journal of Physical Chemistry Letters* **2017**, 3726-3733.

94. Oliveira, L.; Magna, P.; Gallo, N. J. H.; Domenicucci, E. C.; Li, M. S., Coupled Pairs of Cu+OCN^- in KCl Studied by Optical Absorption and Thermally Stimulated Depolarization Current. *physica status solidi (b)* **1992**, 141-151.

95. Yang, W. S.; Noh, J. H.; Jeon, N. J.; Kim, Y. C.; Ryu, S.; Seo, J.; Seok, S. I., High-performance photovoltaic perovskite layers fabricated through intramolecular exchange. *Science* **2015**, 1234.

doi:10.6342/NTU201903018